International Journal of Antennas and Propagation

Substrate Integrated Waveguide (SIW) Based Circuits and Systems

Lead Guest Editor: Arvind Kumar
Guest Editors: Ayman A. Althuwayb and Divya Chaturvedi

Substrate Integrated Waveguide (SIW) Based Circuits and Systems

International Journal of Antennas and Propagation

Substrate Integrated Waveguide (SIW) Based Circuits and Systems

Lead Guest Editor: Arvind Kumar
Guest Editors: Ayman A. Althuwayb and Divya Chaturvedi

Chief Editor

Associate Editors

Academic Editors

Contents

Hindawi
International Journal of Antennas and Propagation
Volume 2023, Article ID 2478853, 8 pages
https://doi.org/10.1155/2023/2478853

Research Article

A Miniaturized Dual-Band Short-Ended ZOR Antenna with Backed Ground Plane for Improved Bandwidth and Radiation Efficiency

Rajkishor Kumar,[1] **Avinash Chandra**,[1] **Sreenath Reddy Thummaluru**,[2] **Mohammad Monirujjaman Khan**,[3] **and Raghvendra Kumar Chaudhary**[4]

[1]*School of Electronics Engineering, Vellore Institute of Technology, Vellore, Tamil Nadu 632014, India*
[2]*Department of Electronics and Communication Engineering, Indian Institute of Information Technology Design and Manufacturing (IIITDM), Kancheepuram, Chennai 600127, India*
[3]*Department of Electrical and Computer Engineering, North South University, Bashundhara, Dhaka-1229, Bangladesh*
[4]*Department of Electrical Engineering, Indian Institute of Technology Kanpur, Kanpur 208016, India*

Correspondence should be addressed to Mohammad Monirujjaman Khan; khandrmohammadmonirujjaman@gmail.com

Received 10 August 2022; Revised 13 September 2022; Accepted 29 November 2022; Published 9 February 2023

Academic Editor: Hervé Aubert

This paper presents a miniaturized planar dual-band short-ended metamaterial antenna with the backed ground plane to improve antenna bandwidths and radiation characteristics. The proposed dual-band metamaterial (MTM) antenna has been made up of the composite right- or left-handed transmission line (CRLH-TL) concept. Here, the backed ground plane has been employed to generate an extra coupling capacitance (C_C), which shifts the ZOR frequency in the lower band while also improving ZOR matching and increasing the impedance bandwidth of the higher-order mode. In this proposed MTM antenna, interdigital capacitance (IDC) has been used in place of a simple series gap, which shifts the higher-order impedance bandwidth into a lower frequency band for second-band Wi-MAX applications (3.3–3.7 GHz). The proposed antenna offers a short-ended MTM, and hence the ZOR frequency is controlled by a series of LC lumped parameters. The proposed antenna offers dual-band behavior with measured −10 dB impedance bandwidths of 5.55% and 41.57% at centered frequencies of 2.70 GHz and 4.33 GHz, respectively. The overall electrical size of the designed antenna is $0.225\lambda_0 \times 0.144\lambda_0 \times 0.0144\lambda_0$ at ZOR ($f_0 = 2.70$ GHz), where λ_0 is the free space wavelength; therefore, it is applicable for different Wi-MAX application bands (2.5–2.7 GHz/3.3–3.8 GHz). Furthermore, the proposed dual-band MTM antenna provides compactness, low loss, stable gain, and radiation efficiency, and also offers omnidirectional radiation patterns in the *E*-plane and dipolar type radiation patterns in the *H*-plane, respectively.

1. Introduction

In a metamaterial antenna, the zeroth-order resonance is a special property derived by plotting the dispersion characteristics of composite right- or left-handed transmission lines (CRLH-TL). In the zeroth-order resonant (ZOR) mode, the physical size of the antenna is independent of the resonant frequency [1–8]. Since metamaterial (MTM) is an artificial structure, it has some unnatural properties, such as group and phase velocities being in opposite directions and a nonlinear progressive phase [9, 10]. Several works have been performed based on the ZOR property to miniaturize the size of the antenna, despite the fact that it has a narrow bandwidth, negative gain, and poor radiation efficiency [11, 12]. In recent years, numerous methods have been introduced to improve the impedance bandwidth, gain, and radiation efficiency of metamaterial antenna [13]. Short-ended MTM antenna offers designed flexibility for the antenna community to control ZOR frequency by varying series parameters [14]. Due to the recent requirement of different wireless communication bands in one system, dual or multiband antennas are more demanding to fulfill these

requirements. The advantages of dual or multiband antennas are that they reduce the number of antennas and space usage and also overcome interference between other frequency bands [15–17]. Many dual-band compact ZOR antennas have been reported in recent years, but these dual-band MTM antennas have suffered from impedance bandwidth peak gain and radiation efficiency [18–22]. So, there are very big challenges for the antenna community to design such a type of dual-band MTM antenna to remove all these drawbacks.

In this context, a compact short-ended CPW-fed ZOR antenna for dual-band applications has been presented. The proposed dual-band MTM antenna improved the ZOR and other higher-order mode impedance bandwidths and radiation efficiencies without affecting its compactness. The designed antenna is basically based on short-ended termination; thus, ZOR frequency depends on LC series parameters and can be controlled by varying series elements of the antenna. Here, an interdigital capacitor is provided, shifting the second resonating frequency towards the lower band. In addition, the backed ground plane improves matching, shifting the frequency on the lower side, and creating wideband nature. The advantages of the proposed antenna are its compactness, low loss, CPW feeding, via-less design, easy fabrication process, low cost, realization of series parameters, and good radiation capacity.

2. Antenna Design Techniques

2.1. Composite Left- and Right-Handed Transmission Line (CRLH-TL) Theory. Figure 1 shows an equivalent circuit diagram of the proposed dual-band MTM antenna. It consists of left-handed shunt inductance L_L, right-handed series inductance L_R, left-handed series capacitance C_L, and right-handed shunt capacitance C_R. As per the CRLH-TL theorem, the resonance frequencies have been found using these four CRLH-TL parameters (L_L, L_R, C_L, and C_R), and they are independent of the size of the antenna.

From the Bloch and Floquet theory, the dispersion relation is determined for the unit cells of periodic structures, and it is reported in [9, 10].

$$\beta_{\mathrm{CRLHTL}}(\omega) = \frac{1}{p}\cos^{-1}\left[1 + \frac{Z_{\mathrm{CRHL}}(\omega) \times Y_{\mathrm{CRLH}}(\omega)}{2}\right], \quad (1)$$

where

$$Z_{\mathrm{CRLH}}(\omega) = j\left(\omega L_R - \frac{1}{\omega C_L}\right),$$

$$Y_{\mathrm{CRLH}}(\omega) = j\left(\omega C_R - \frac{1}{\omega L_L}\right)\text{Without backed ground plane}, \quad (2)$$

$$Y_{\mathrm{CRLH}}(\omega) = j\left(\omega C_R + \omega C_c - \frac{1}{\omega L_L}\right)\text{With backed ground plane}.$$

Here, the phase constant (β) is related to the Bloch wave, and p shows the unit cell length of the proposed dual-band MTM antenna.

The resonance frequency of the designed CRLH-TL based on a dual-band MTM has been found using the given equation

$$\beta_n p = \frac{n\pi p}{l} = \frac{n\pi}{N}\ (n = 0, 1, 2, 3, 4, \ldots\ldots\ldots\ldots, (N-1), \quad (3)$$

where l (=Np), n, and N are the length of the resonator, the resonance modes, and the unit cell number.

The designed dual-band MTM antenna is based on short-ended boundary conditions; therefore, the input impedance (Z_{in}) is found from one side of the resonator towards the other side, whereas the load impedance is zero ($Z_L = 0$). So, the input impedance (Z_{in}) is obtained by [9]

$$Z_{\mathrm{in}}^{\mathrm{short}} = -jZ_0 \times \tan(\beta l) \sim jZ_0 \times \beta l = j\sqrt{Z'_{\mathrm{CRLH}}/Y'_{\mathrm{CRLH}}}\left(\frac{\sqrt{Z'_{\mathrm{CRLH}}Y'_{\mathrm{CRLH}}}}{j}\right)l = Z'_{\mathrm{CRLH}} \times l = Z \times Np, \quad (4)$$

where Z_0 is the characteristic of CRLH-TL, Z'_{CRLH} and Y'_{CRLH} are the series impedance and shunt admittance per unit periodic length.

When $n = 0$ (from (3)), the propagation constant $\beta = 0$ shows the ZOR mode, and the resonance frequency is obtained by

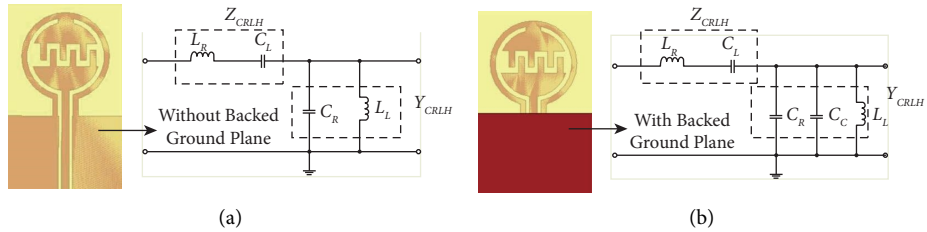

FIGURE 1: Equivalent circuit diagram (a) without backed ground plane, and (b) with backed ground plane of the proposed dual-band MTM antenna.

$$\omega_{se} = \omega_{ZOR} = \frac{1}{\sqrt{L_R C_L}}. \quad (5)$$

From (5), the ZOR frequency has been contained by variation of series capacitance (C_L) and inductance (L_R) of the proposed dual-band MTM.

2.2. Antenna Configuration. The configuration of the proposed dual-band MTM antenna is shown in Figure 2. The proposed MTM antenna has been fabricated on an FR4 glass-epoxy substrate ($\varepsilon_r = 4.4$, $\tan\delta = 0.02$) with a compactness of 1.6 mm.

It consists of a circular patch having an interdigital capacitor, a CPW ground plane, and a partially backed ground plane. The designed MTM antenna is fed by a 50 Ω microstrip line. The interdigital capacitance forms a series capacitor (C_L), while the small stripline acts as a shunt inductor (L_L), which verifies the composite right- or left-handed transmission line-based MTM. C_C is the coupling capacitance between the CPW feed and the partially backed ground plane, whereas C_R is the shunt capacitance obtained between the upper ground plane and the CPW feed. The series inductance (L_R) is realized by a signal patch. The overall electrical size of a designed dual-band MTM antenna is $0.225\lambda_0 \times 0.144\lambda_0 \times 0.0144\lambda_0$ at ZOR ($f_0 = 2.70$ GHz), where λ_0 is the free space wavelength.

2.3. Validation of ZOR Mode. To verify the short-ended condition of ZOR frequency, parametric analysis has been done based on the series element, i.e., L_R. Figure 3 shows the input reflection coefficient with different values of patch width called series inductor (L_R) with respect to frequency. It is found that ZOR frequency decreases towards the lower frequency band when patch width (W_F) increases, which confirms the behavior of ZOR mode. There is another way to verify the ZOR conditions of the proposed antenna by plotting the electric field at ZOR frequency. It is clearly observed from Figure 4 that the distributions of the electric field are showing in phase at 2.72 GHz. Therefore, it verified the ZOR condition occurred at a 2.72 GHz resonance frequency.

2.4. Effect of Backed Ground Plane. In this subsection, the effect of with and without backed ground plane on the input reflection coefficient has been demonstrated. It is observed from Figure 5 that, due to the backed ground plane, one more coupling capacitance (C_C) is introduced to shift the ZOR frequency from 3.3 to 2.72 GHz and also improve the higher-order impedance bandwidth of the designed antenna. This coupling capacitance helps to miniaturize the size of the antenna as well as the backed ground plane coupled with the radiator to improve the matching and enhanced impedance bandwidth.

2.5. Effect of Series Gap and Interdigital Capacitance. Here, the effect of the series gap and interdigital capacitance on the reflection coefficient has been studied, as shown in Figure 6. The spiral-shaped is nothing but interdigital capacitance, which provides more capacitive values compared with the inductive values in order to get good performance at the lower band of the proposed antenna structure. It is clearly observed from Figure 6 that the interdigital capacitance provides a better response compared to series gap capacitance and shifts the impedance bandwidth frequency to the lower side.

3. Simulated and Measured Results

A prototype antenna has been fabricated to verify the measured and simulated near- and far-field results, as shown in Figure 7. The Keysight programmable network analyzer (N5221A) has been used to measure near-field results, i.e., the input reflection coefficient. The simulated dual-band MTM antenna offers −10 dB input impedance bandwidth of 5.14% (2.65–2.79 GHz) and 30.37% (3.63–4.93 GHz) for the first and second bands, respectively, whereas the measured −10 dB input impedance bandwidth ($S_{11} < -10$ dB) offers 5.55% (2.63–2.78 GHz) and 41.57% (3.43–5.23 GHz) for the first and second band, respectively, as shown in Figure 8. The simulated and measured resonant frequency of ZOR is found to be 2.72 GHz and 2.70 GHz, respectively, and also higher-order impedance bandwidth increases. This happens due to imperfections in antenna fabrication and tolerance in soldering.

Figure 9 illustrates the normalized radiation patterns of the proposed antenna in the *xz*- and *yz*-plane at 2.72 GHz and 4.58 GHz, respectively. It is observed that at ZOR frequency (2.72 GHz) and 4.58 GHz, the proposed antenna shows an omnidirectional radiation pattern in the *xz*-plane. At frequencies 2.72 GHz and 4.58 GHz, it shows a dipolar type radiation pattern in *yz*-plane. The difference between copolarization and cross-polarization levels in the *xz*-plane is −46.53 dB at 2.72 GHz and −40.03 dB at 4.58 GHz.

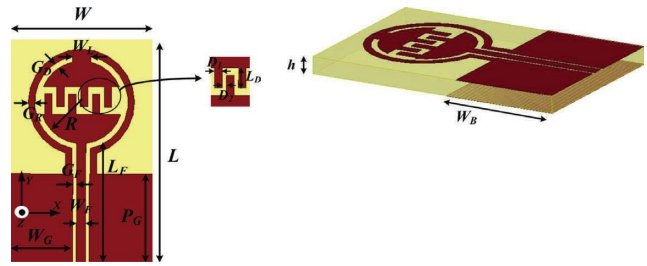

Figure 2: Geometry of proposed dual-band metamaterial antenna ($L = 25$, $W = 16$, $P_G = 10$, $W_G = 7.1$, $W_F = 1$, $G_F = 0.4$, $L_F = 13.5$, $R = 4.5$, $G_R = 0.7$, $G_D = 0.6$, $W_L = 2$, $D_1 = 0.8$, $D_2 = 0.5$, $L_D = 2.2$, $W_B = 11$, $h = 1.6$: all dimensions are in mm).

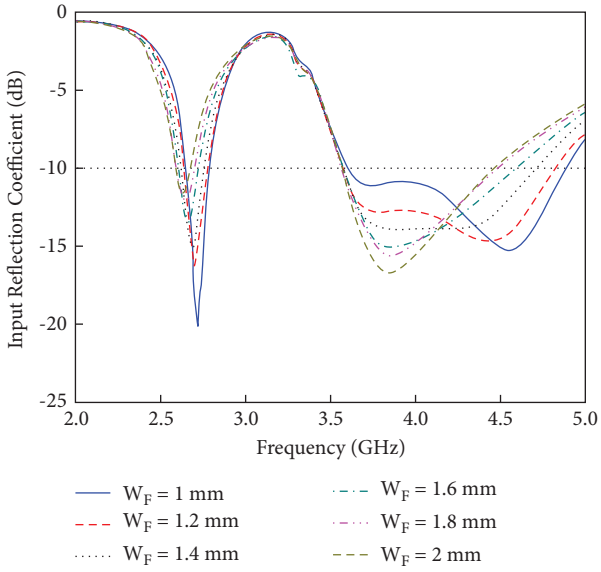

Figure 3: Simulated reflection coefficient of the proposed dual-band MTM antenna by varying W_{F3}.

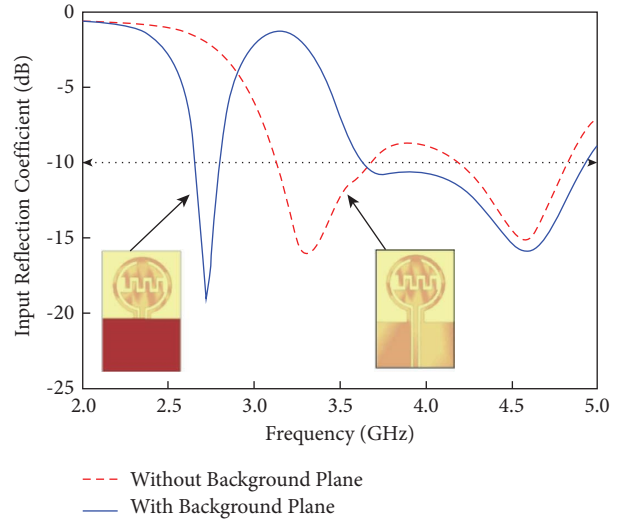

Figure 5: Input reflection coefficient of proposed dual-band MTM with and without backed ground plane.

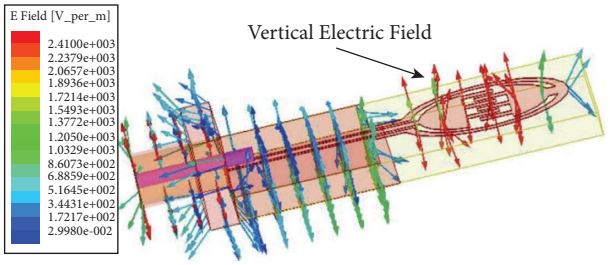

Figure 4: Electric field distribution to confirm the ZOR mode at 2.72 GHz.

The maximum gain of the proposed dual-band MTM antenna is 0.72 dBi for the first band and 2.0 dBi for the second band, respectively, whereas it shows a measured maximum peak gain of 0.59 dBi for the first band and 2.10 dBi for the second band, respectively [23], as shown in Figure 10(a). The designed dual-band MTM antenna shows an average radiation efficiency of 71.52% for the first band

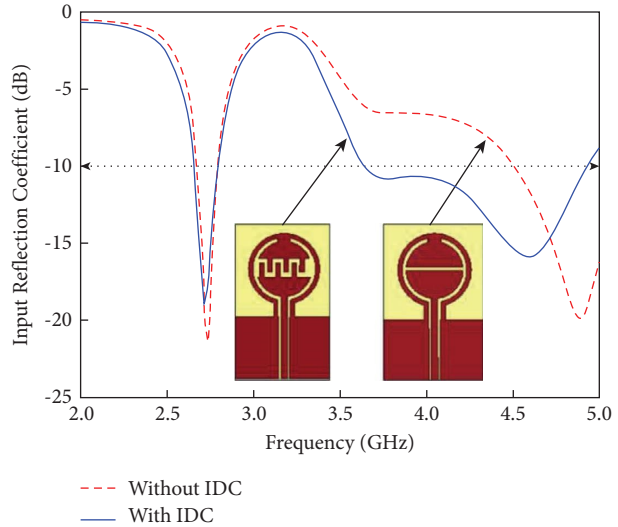

Figure 6: Input reflection coefficient of proposed dual-band MTM with and without IDC.

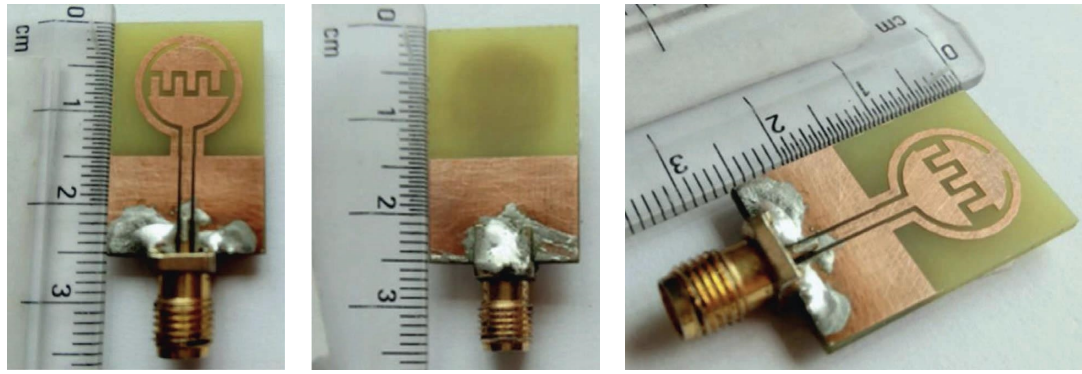

Figure 7: Photograph of proposed dual-band MTM antenna: (a) top view, (b) ground plane, and (c) 3D view.

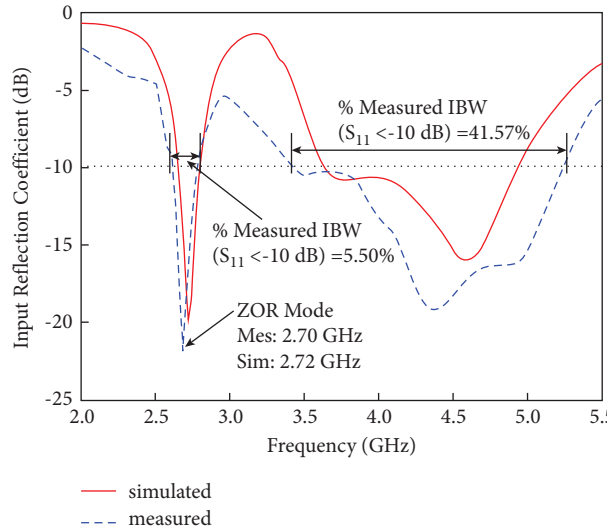

Figure 8: Simulated and measured input reflection coefficients of the proposed dual-band MTM antenna.

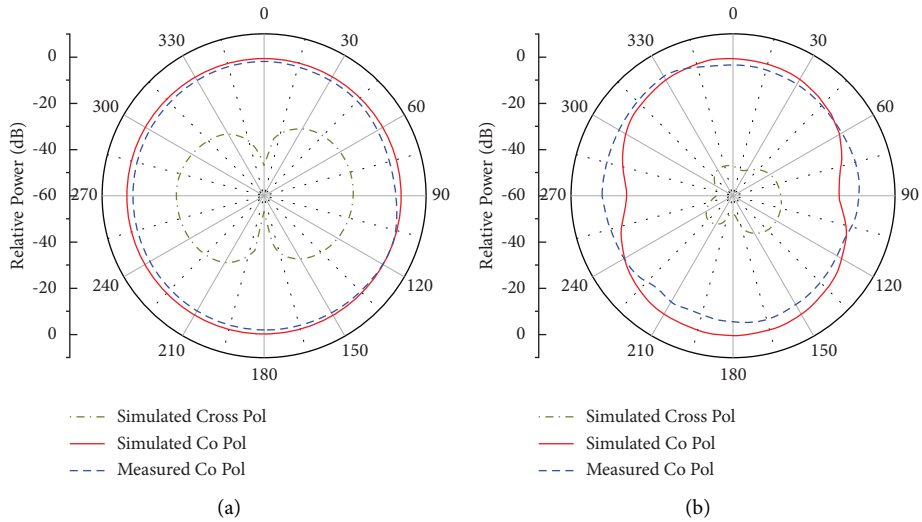

Figure 9: Continued.

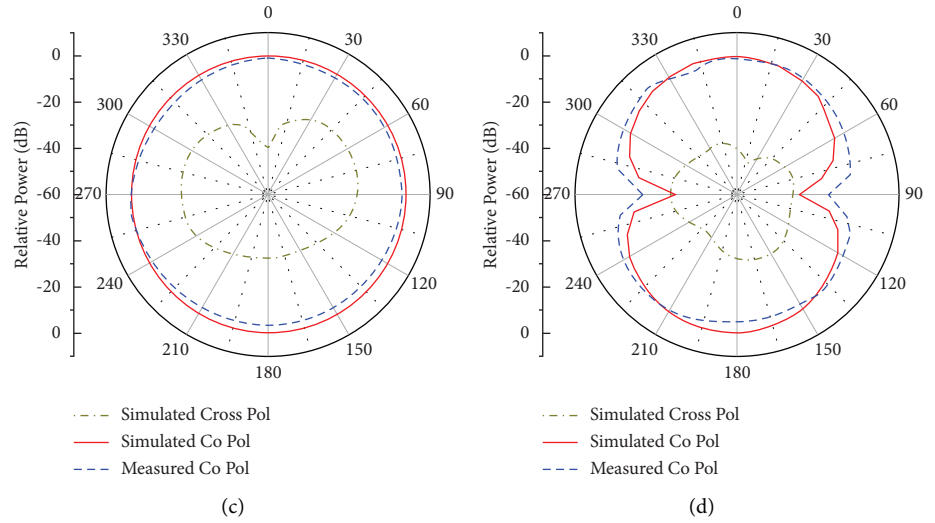

Figure 9: Normalized radiation patterns: (a) *xz*-plane, 2.72 GHz; (b) *yz*-plane, 2.72 GHz; (c) *xz*-plane, 4.58 GHz; (d) *yz*-plane, 4.58 GHz of proposed dual-band MTM antenna.

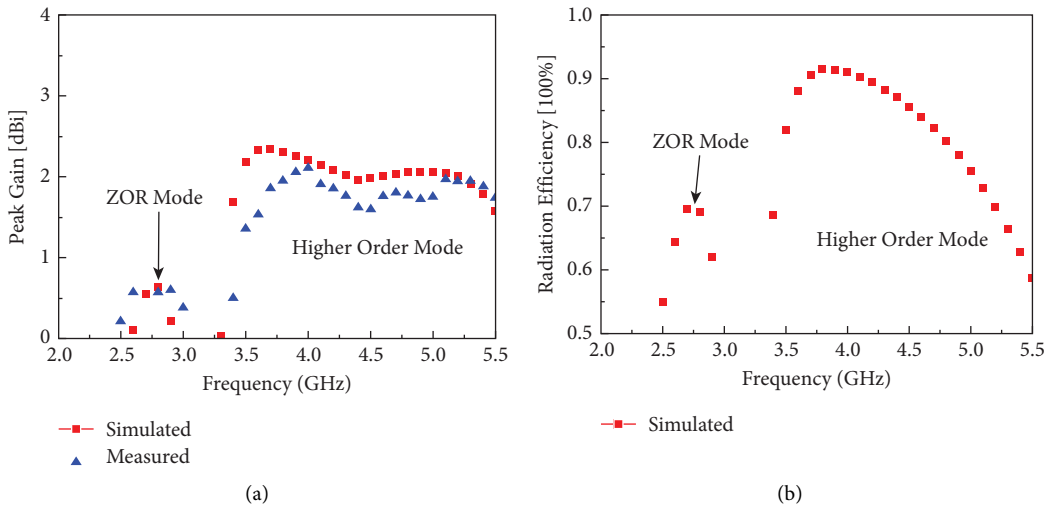

Figure 10: Far-field results of proposed dual-band MTM antenna in the broadside direction. (a) Simulated and measured gain; (b) radiation efficiency.

Table 1: Comparison of dual-band MTM antennas with recently published work.

Ref.	Antenna size	Resonance frequency (GHz)	Via process	−10 dB impedance bandwidth (%)	Gain (dBi)	Radiation efficiency (%)
[13]	$0.27\lambda_0 \times 0.23\lambda_0$	2.6/3.6	Not needed	2.29/28.57	0.53/1.98	NA#/NA#
[16]	$0.33\lambda_0 \times 0.098\lambda_0$	2.45/3.37	Not needed	8.16/23.74	0.3/1.1	68/77.3
[24]	$1.05\lambda_0 \times 1.05\lambda_0$	6.6/10.9	Needed	3.03/5.04	7.29/2.97	NA#/NA#
[25]	$1.27\lambda_0 \times 1.27\lambda_0$	1.73/5.36	Not needed	17.34/11.75	8.23/8.30	NA#/NA#
[26]	$0.021\lambda_0 \times 0.018\lambda_0$	0.91/2.45	Needed	17.8/35.8	−17.1/ −9.81	NA#/NA#
[27]	$0.35\lambda_0 \times 0.45\lambda_0$	2.58/5.41	Not needed	20.6/15.7	3.5/3.53	NA#/NA#
PW*	$0.22\lambda_0 \times 0.14\lambda_0$	2.72/4.58	Not needed	5.50/41.57	0.72/2.0	71.52/84.02

NA# = not available, PW* = proposed work.

and 84.02% for the second band, as shown in Figure 10(b). Table 1 shows the comparison among dual-band MTM antennas with recently published work. It is observed that the advantages of the proposed dual-band MTM antenna are an overall improvement in impedance bandwidth, a high level of miniaturization, and via-less design.

4. Conclusion

A miniaturized CPW-fed dual-band short-ended ZOR-based antenna with the backed ground plane is investigated. The proposed antenna is short-ended, so the ZOR mode is dependent upon the series LC parameters of the proposed MTM antenna. The designed antenna consists of the backed ground plane to introduce extra capacitance, which is used to shift ZOR frequency towards a lower frequency band and miniaturize the size of the antenna. Here, instead of a series gap, an interdigital capacitance is used in the proposed antenna to lower the higher-order impedance bandwidth. The designed antenna offers dual-band behavior with measured −10 dB impedance bandwidths of 5.55% (centered at 2.70 GHz) and 41.57% (centered at 4.33 GHz) for the first and second bands, respectively. The proposed antenna shows a measured maximum peak gain of 0.59 dBi for the first band and 2.10 dBi for the second band, respectively, whereas it shows an averaged simulated radiation efficiency of 71.52% and 84.02% for the first and second bands, respectively. Furthermore, the proposed MTM offers a high level of compactness and an omnidirectional and dipolar type radiation pattern, which is suitable for Wi-MAX band applications.

Data Availability

The data that support the findings of this study are available from the corresponding author upon reasonable request.

Conflicts of Interest

The authors declare that there are no conflicts of interest regarding the publication of this paper.

References

[1] J. Fu and O. H. Raheem, "A novel IMSL tunable phase shifter for HMSIW-LWA-fed rectangular patches based on nematic liquid crystal," *Applied Physics A*, vol. 123, no. 7, pp. 493–498, 2017.

[2] A. Kumar and S. Imaculate Rosaline, "Hybrid half-mode SIW cavity-backed diplex antenna for on-body transceiver applications," *Applied Physics A*, vol. 127, no. 11, pp. 834–837, 2021.

[3] D. Chaturvedi, A. A. Althuwayb, and A. Kumar, "Bandwidth enhancement of a planar SIW cavity-backed slot antenna using slot and metallic-shorting via," *Applied Physics A*, vol. 128, no. 3, pp. 193–2022, 2022.

[4] L. Fagiolari, E. Varaia, N. Mariotti, M. Bonomo, C. Barolo, and F. Bella, "Poly (3, 4-ethylenedioxythiophene) in dye-sensitized solar cells: toward solid-state and platinum-free photovoltaics," *Advanced Sustainable Systems*, vol. 5, no. 11, Article ID 2100025, 2021.

[5] A. A. Althuwayb, "SIW cavity-backed slot antenna with monopole-like radiation for vehicular communications," *Applied Physics A: Materials Science & Processing*, vol. 202, 2022.

[6] A. Sanada, C. Caloz, and T. Itoh, "Novel zeroth order resonance incomposite left/right handed transmission line resonators," in *Proceedings of the Asia-Pacific Microwave Conference*, pp. 1588–1591, Seoul, Korea, November 2003.

[7] R. W. Ziolkowski and A. Erentok, "Metamaterial-based efficient electrically small antennas," *IEEE Transactions on Antennas and Propagation*, vol. 54, no. 7, pp. 2113–2130, 2006.

[8] S. K. Sharma, A. Gupta, and R. K. Chaudhary, "Epsilon negative CPW-fed zeroth-order resonating antenna with backed ground plane for extended bandwidth and miniaturization," *IEEE Transactions on Antennas and Propagation*, vol. 63, no. 11, pp. 5197–5203, 2015.

[9] C. Caloz and T. Itoh, *Electromagnetic Metamaterials: Transmission Line Approach and Microwave Applications*, Wiley, Hoboken, NJ, USA, 2005.

[10] B. D. Bala, M. K. A. Rahim, and N. A. Murad, "Composite right/left-handed dual-band metamaterial antenna with improved gain and efficiency," *Microwave and Optical Technology Letters*, vol. 56, no. 7, pp. 1575–1579, 2014.

[11] A. Lai, K. M. K. H. Leong, and T. Itoh, "Infinite wavelength resonant antennas with monopolar radiation pattern based on periodic structures," *IEEE Transactions on Antennas and Propagation*, vol. 55, no. 3, pp. 868–876, 2007.

[12] T. Jang, J. Choi, and S. Lim, "Compact Coplanar Waveguide (CPW)-Fed Zeroth-Order Resonant antennas with extended bandwidth and high efficiency on vialess single layer," *IEEE Transactions on Antennas and Propagation*, vol. 59, no. 2, pp. 363–372, 2011.

[13] P.-L. Chi and Y.-S. Shih, "Compact and bandwidth-enhanced Zeroth order resonant antenna," *IEEE Antennas and Wireless Propagation Letters*, vol. 14, pp. 285–288, 2015.

[14] A. Gupta and R. Kumar Chaudhary, "A compact short-ended zor antenna with gain enhancement using ebg loading," *Microwave and Optical Technology Letters*, vol. 58, no. 5, pp. 1194–1197, 2016.

[15] A. Mehdipour, T. A. Denidni, and A. R. Sebak, "Multi-band miniaturized antenna loaded by ZOR and CSRR metamaterial structures with monopolar radiation pattern," *IEEE Transactions on Antennas and Propagation*, vol. 62, no. 2, pp. 555–562, 2014.

[16] R. Samson Daniel, R. Pandeeswari, and S. Raghavan, "A compact metamaterial loaded monopole antenna with offset-fed microstrip line for wireless applications," *AEU - International Journal of Electronics and Communications*, vol. 83, pp. 88–94, 2018.

[17] T. Ali, A. Mohammad Saadh, R. C. Biradar, J. Anguera, and A. Andújar, "A miniaturized metamaterial slot antenna for wireless applications," *AEU - International Journal of Electronics and Communications*, vol. 82, pp. 368–382, 2017.

[18] L.-M. Si, W. Zhu, and H.-J. Sun, "A compact planar and CPW-fed metamaterial-inspired dual-band antenna," *IEEE Antennas and Wireless Propagation Letters*, vol. 12, pp. 305–308, 2013.

[19] B. Zong, G. Wang, C. Zhou, and Y. Wang, "Compact low-profile dual-band patch antenna using novel TL-MTM structures," *IEEE Antennas and Wireless Propagation Letters*, vol. 14, pp. 567–570, 2015.

[20] B. P. Smyth, S. Barth, and A. K. Iyer, "Dual-band microstrip patch antenna using integrated uniplanar metamaterial-based

EBGs," *IEEE Transactions on Antennas and Propagation*, vol. 64, no. 12, pp. 5046–5053, 2016.

[21] S. K. Sharma, M. A. Abdalla, and R. K. Chaudhary, "An electrically small SICRR metamaterial-inspired dual-band antenna for WLAN and WiMAX applications," *Microwave and Optical Technology Letters*, vol. 59, no. 3, pp. 573–578, 2017.

[22] R. Kumar, R. Singh, and R. K. Chaudhary, "Miniaturised triple-band antenna loaded with complementary concentric closed ring resonators with asymmetric coplanar waveguide-fed based on epsilon negative transmission line," *IET Microwaves, Antennas & Propagation*, vol. 12, no. 13, pp. 2073–2079, 2018.

[23] C. J. Brochu, G. A. Morin, and J. W. Moffat, "Gain measurement of a cavity-backed spiral antenna from 4 to 18 GHz using the three-antenna method," *Defence Research Establishment Ottawa (ONTARIO)*, ADA359308, 1998.

[24] R. Jie, H. Jing, S. Li, and Y. Xiao, "Dual-band circular polarizers based on a planar chiral metamaterial structure," *IEEE Antennas and Wireless Propagation Letters*, vol. 18, no. 12, pp. 2587–2591, 2019.

[25] W. Kamonsin, P. Krachodnok, P. Chomtong, and P. Akkaraekthalin, "Dual-band metamaterial based on jerusalem cross structure with interdigital technique for LTE and WLAN systems," *IEEE Access*, vol. 8, pp. 21565–21572, 2020.

[26] M. Zada, I. A. Shah, and H. Yoo, "Metamaterial-Loaded compact high-gain dual-band circularly polarized implantable antenna system for multiple biomedical applications," *IEEE Transactions on Antennas and Propagation*, vol. 68, no. 2, pp. 1140–1144, 2020.

[27] X. Wu, X. Wen, J. Yang, S. Yang, and J. Xu, "Metamaterial structure based dual-band antenna for WLAN," *IEEE Photonics Journal*, vol. 14, no. 2, pp. 1–5, Article ID 7722105, 2022.

Hindawi
International Journal of Antennas and Propagation
Volume 2022, Article ID 4151038, 9 pages
https://doi.org/10.1155/2022/4151038

Research Article

Design of Dual-Band, 4-Ports MIMO Antenna-Diplexer Based on Quarter-Mode Substrate Integrated Waveguide

Mansour H. Almalki, Adnan Affandi, and Avez Syed

Electrical and Computer Engineering Department, Faculty of Engineering, King Abdulaziz University, P.O. Box 80204, Jeddah 21589, Saudi Arabia

Correspondence should be addressed to Avez Syed; avez.ssyed@gmail.com

Received 14 August 2022; Accepted 10 September 2022; Published 23 September 2022

Academic Editor: Arvind Kumar

Here, a compact, dual band, 4-elements multi-input and multi-output (MIMO) antenna diplexer is designed to use in wireless local area network (WLAN) applications. The antenna is accomplished in a planar profile by employing Substrate Integrated Waveguide (SIW) technology. To reduce the size of a single element by 75%, a quarter-mode substrate integrated waveguide (QMSIW) technology is introduced. The QMSIW is realized by bisecting the full-mode SIW along the two magnetic walls and considering the quarter-mode for the operation. Initially, two-QMSIW cavities of distinct dimensions are designed to operate in two frequency bands, 5.2 GHz and 5.8 GHz, respectively. Later, two more radiating elements operating at the same frequencies are integrated with a 2-elements antenna. For better polarization decoupling, the identical elements are placed perpendicular to each other, and a parasitic metallic strip loaded with shorting vias is placed between two identical frequency antenna elements; hence, the port isolation is improved up to −25 dB. The antenna covers a bandwidth of 1.8% in the lower frequency band while 2.2% in the upper frequency band. The antenna prototype is fabricated, and its results are verified with experimental data. It is observed that the measured results are closely following the simulated results.

1. Introduction

Wireless communication channel environment is a densely populated area as the links are more susceptible to fading and co-channel interference, hence, due to this reason, power falls substantially with space. Thus, it becomes challenging for the antenna designer to design a system with higher spectral efficiency, higher quality of service, and wide bandwidth [1–4]. Therefore, the wireless communication parameters in a complex setting can be enhanced by employing spatial multiplexing and diversity techniques. Multiplexing techniques mainly improve the channel capacity, which leads to enhanced data rate, while diversity techniques improve the reliability of communication. Thus, the MIMO antenna is an optimum alternative to mitigate the fading by employing receiver and transmit diversity. In the modern world, electronic devices are dropping in size every day; thus, there is a need for a compact system. In this concern, the antenna plays a vital role. The next stringent requirement is good isolation levels between the radiating elements because they are very close to a compact structure. There are various techniques suggested by the researchers to enhance the isolation level [5–9]. In [5], photonic band gap structures are placed between transmitting and receiving antennas, a metamaterial mushroom structure is used between 4 closed-spaced antennas in [6], two cross-neutralization lines are used in [7], and a meandering slot along with an inverted *T* slot is etched in the ground plane in [8].

In the past two decades, Substrate Integrated Waveguide (SIW) based cavity-backed antennas have played a vital role in developing self-diplexing antennas [9–11]. The overall size of the SIW antenna can be substantially condensed by retaining similar bandwidth and radiation characteristics by employing half-mode (HM) SIW [12–14], quarter-mode (QM) SIW [15], and eight mode (EM) SIW [16] topologies. Many multiple antenna systems were

investigated [17–25]. However, only a few of them discussed the MIMO properties. In [17], the dual-band performance is realized by coupling a parasitic rectangular patch with the HMSIW cavity; however, the antenna suffers from narrow bandwidth. To improve bandwidth with compact size, the HMSIW cavities are loaded with rectangular slots to split the dominant mode into odd- and even-half modes [18]. To improve the bandwidth and gain in each operating band, a half-split cylindrical dielectric resonator is realized in [19]. To realize a small dual-band MIMO antenna, a split ring resonator (SRR) slot is employed, but the isolation level in the inter-elements becomes poor [20].

In this article, a dual-band 4-elements-self-diplexing MIMO antenna is developed to operate in the lower frequency band around 5.2 GHz (5.15–5.26 GHz, 110 MHz) and the higher frequency band around 5.8 GHz (5.75–5.88 GHz, 130 MHz) for wireless local area network (WLAN) bands. The size of the proposed design is minimized to a quarter by employing the QMSIW cavity. The proposed MIMO antenna has potential use in enhancing data transmission speed by twice compared to a 2-elements antenna. In a complex communication environment, this antenna also can be considered to improve the reliability of data links. The MIMO properties of a 2×2 elements antenna diplexer have been evaluated in terms of the Envelop Correlation Coefficient (ECC) and diversity gain (DG). The exclusive and modest proposed antenna shape maintains isolation between any two ports below −25 dB just by employing rectangular metallic strips loaded with shorting vias. Both the lower and upper resonant frequencies can be scaled individually by altering the QMSIW cavity length. This article is divided into three sections. Section 2 presents the design methodology of a 4-elements self-diplexing MIMO antenna system, Section 3 presents simulated and measured results, and Section 4 has concluded the proposed idea.

2. 4-Ports Self-Diplexing Antenna Design Process

Figure 1 shows the geometrical view of the proposed QMSIW cavity-backed slot antenna. The various stages used in the design progression from the full-mode SIW to the QM SIW cavity resonators are explained in Figure 2. The design of the proposed antenna is modeled with the help of a Computer Simulation Technology (CST) Microwave studio simulator [11]. The first step is calculating the dominant mode resonant frequency of the rectangular cavity at around 5.2 GHz using (1) [12]. The dimensions of the rectangular cavity are evaluated as $27.4 \times 27.4\ \text{mm}^2$. The QMSIW cavity is achieved by firstly bisecting the FMSIW cavity along two magnetic walls, then preserving the quarter-part of the full-dominant mode. By using the abovementioned steps, two QM planar cavities are designed where the first cavity (i.e., Cav1) operates at 5.2 GHz and the second cavity (i.e., Cav2) operates at 5.8 GHz, as shown in Figure 2(a). The operating frequency equation for the FMSIW cavity can be calculated using (1) [9, 15] shown below.

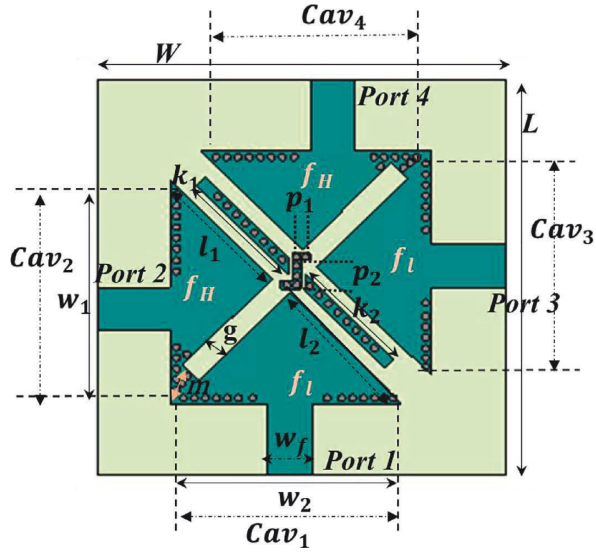

Figure 1: Schematic diagram of 4-ports self-diplexing antenna (dimensions, $w_1 = w_2 = 25$, $l_1 = 15.7$, $l_2 = 17.4$, $g = 2.5$, $w_f = 5$, $k_1 = k_2 = 16$, $p_1 = 1.6$, $m_2 = 3.2$, d = 0.8, s = 1.6, $L = W = 44.2$) (unit: mm).

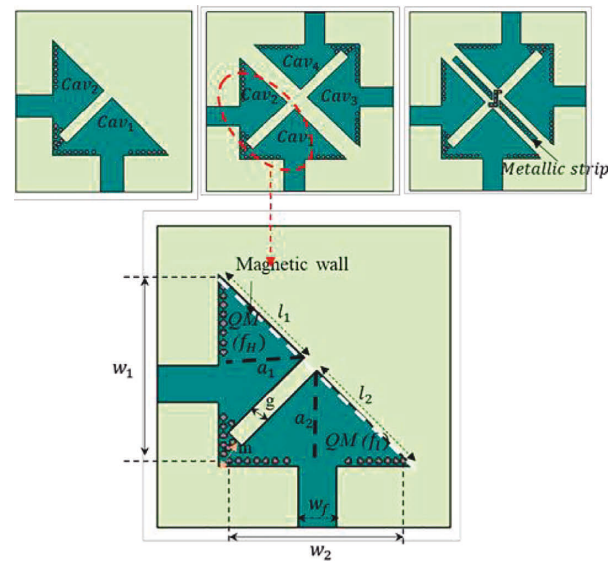

Figure 2: Design evolution to accomplish a dual element 4-ports antenna-diplexer.

$$f_{110}(\text{FM}) = \frac{c}{2\sqrt{\varepsilon_{reff}}}\sqrt{\left(\frac{1}{W_{eff}}\right)^2 + \left(\frac{1}{l_{eff}}\right)^2}, \tag{1}$$

where l_{eff} or $W_{eff} = W$ or $L - 1.08\,d^2/p$, w_{eff} and l_{eff} are the effective width and length of the full-mode cavity, d is the diameter, and s is the pitch distance between two shorting vias. The electric walls on each side of the SIW cavity are accomplished by inserting the number of shorting vias, which attach the top and bottom planes of the metallic cladding. In the proposed design, firstly a full-mode SIW is divided into two equal parts along the magnetic walls to

achieve a half-mode (HM) SIW. In the next step, the HMSIW cavity resonator operating in the dominant mode is split into two unequal parts by carving one open-end tilted rectangular slot. Necessarily, this slot translates the HMSIW cavity resonator into two patchy quarter-mode like cavity structures. The QMSIW conserves the lowest operating mode of FMSIW due to its uniform and symmetrical field distribution. 50 Ω microstrip line is adopted for excitation. Each QM cavity operates at a different resonant frequency due to unequal size. To realize better impedance matching characteristics, feed location can be optimized. Three metallic vias, covering a distance of "m," are implanted near the short end of the slot to reduce the inter-element mutual coupling. The dimensions of the QMSIW cavities are optimized to achieve a lower frequency band of around 5.2 GHz and an upper-frequency band of around 5.8 GHz. The final dimensions of this design are tabulated in Table 1 and are symbolized in Figure 1. To achieve a complete planar configuration, microstrip feed line techniques are used to feed the QM cavities. The feed characteristic impedance and the antenna input impedance are matched by optimizing the location of the feed. To avoid leakage loss through vias, the diameter and spacing between the shorting vias are obtained using the design guidelines mentioned in [12]. The 2-element antenna illustrates adequate isolation of around −25 dB between two cavities, as shown in Figure 3. A MIMO diplexing antenna system is achieved by replicating two more similar elements [19]. However, after adding the elements, there is no variation in the reflection coefficient parameters, but the isolation level (S_{ij}) is degraded by around 5 dB.

The design executes the operating bandwidth of around 1.8% in a lower frequency band and 2.2% in an upper-frequency band. The operating principle of the 2-port diplexing antenna is demonstrated in Figure 2. When *Cav1* is fed with microstrip feed while *Cav2* is terminated with a 50 Ω matched termination, the *Cav1* resonates at 5.2 GHz due to its quarter fundamental mode TE110, as presented in [15]. Similarly, when *Cav2* is fed with microstrip feed and Cav1 is ended with matched termination, *Cav2* operates at 5.8 GHz. To reduce the port decoupling, the cavities operating at the same resonant frequency are placed orthogonal to each other. Thus, inherent isolation is achieved at around −20 dB, as shown in Figure 4. However, the isolation level is insufficient for high-powered wireless communication. Furthermore, to improve the isolation.

Rectangular parasitic metallic strips loaded with shorting vias are placed among the QM cavities. The parasitic strips reduce mutual coupling between the cavities of distinct resonant frequencies, which are oriented parallel to each other. The shorting vias make the electric wall by making the electric field zero. Thus, the inter-element isolation levels are getting improved and obtained −25 dB. Figure 5 illustrates clearly how the metallic strip plays an essential role in reducing the field coupling. The scalar electric field plots have been shown in Figure 6(a) without metallic strips and Figure 6(b) including metallic strips. The E-field plots are presented at each operating frequency when the corresponding port is excited. It can be observed in Figure 6(b)

Table 1: The dimensions of the antenna structure. All dimensions are in millimeters (Mm).

w_1	w_2	l_1	l_2	g
25	25	15.7	17.4	2.5
w_f	k_1	k_2	p_1	m_2
5	16	16	1.6	3.2
d	s	L	W	h
0.8	1.6	44.2	44.2	1.57

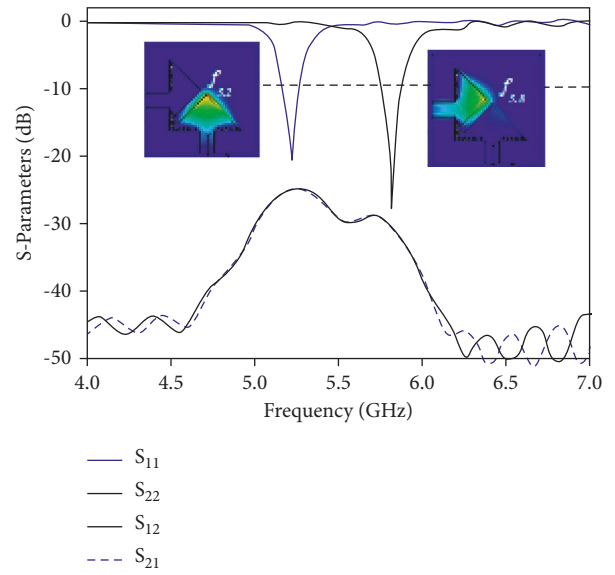

Figure 3: *S*-parameters of dual-band dual element diplexing antenna.

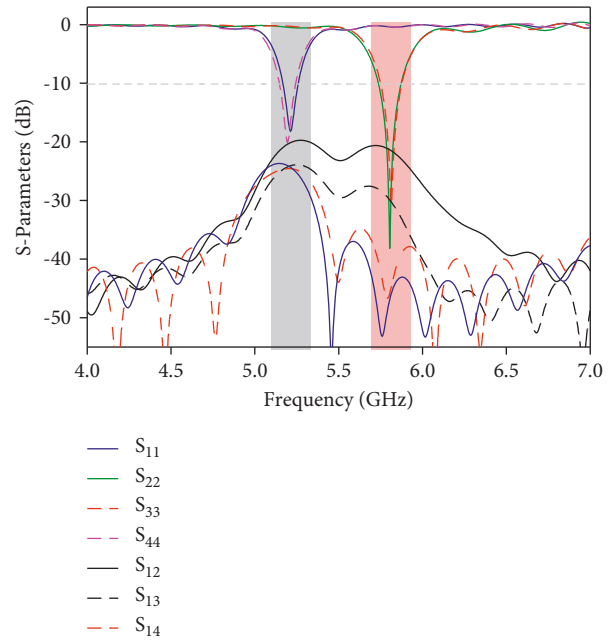

Figure 4: S-parameters of dual-band quad elements diplexing antenna without a metallic strip.

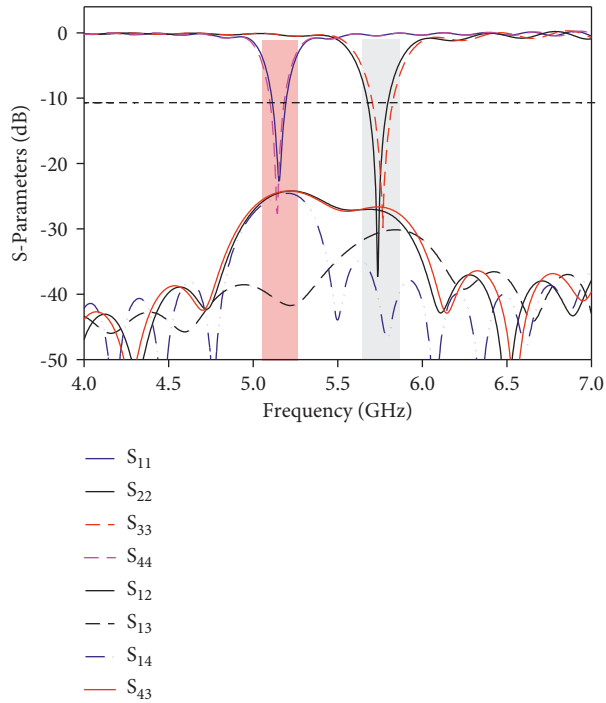

Figure 5: *S*-parameters of dual-band quad elements diplexing antenna with a metallic strip.

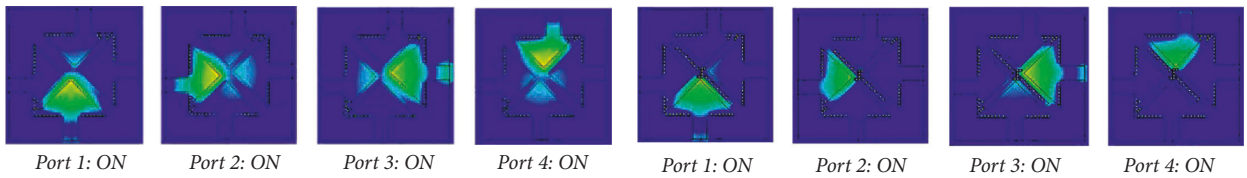

Figure 6: Scalar E-field when corresponding port is powered (a) without parasitic metallic strips (b) with metallic strips.

that mutual coupling with other elements can be reduced significantly.

The operating frequencies of a 4-element diplexing antenna configuration can be rescaled for different bands by simply altering the length of the cavities. It can be observed in Figure 7 that by varying the length a1 of Cav1 in the range of 11.8–12.4 mm, the resonant frequencies can be tuned from 5.3–5.1 GHz. Similarly, it can be observed in Figure 8 that by varying the length a2 of Cav2 in the range of 10.8–11.4 mm, the corresponding resonant frequency can be tuned in the frequency range of 5.9–5.7 GHz.

The resonant frequency can be adjusted individually in both operating bands in a straightforward manner. The scaling of one resonance has no impact on another resonance, which proves the flexibility of the MIMO-antenna system. This antenna design maintains the ground plane integrity, which makes it easy to integrate with other elements. All radiating elements are placed on the top plane. All four cavities share the same ground, making the design simpler and more compact.

2.1. MIMO Properties of Self-Diplexing Antenna. The MIMO features of the proposed design are verified in terms of envelope correlation coefficient (ECC) and diversity gain (DG). ECC governs the correlation in radiation patterns between two independent antennas [8]. Typically, its value should be <0.5. The ECC can be derived from *S*-parameters and far-field gain. The ECC from S-parameters can be extracted from (2). The ECC performance of the proposed design is shown in Figure 9. When *Port-1* and *Port-3* are fed with a microstrip feed line while *Port-2* and *Port-4* are ended with the matched terminations, the peak value of ECC is observed as 0.02. On the other hand, when Port-2 and *Port-4* are fed and the rest are terminated with matched loads, the peak value of ECC is obtained as 0.03. The ECC can be evaluated from *S*-parameters using (2) [19] when *Port-1* and *Port-3* are excited.

$$ECC = \frac{\left|S_{11*}S_{13} + S_{13} * S_{33}\right|^2}{\left(1 - \left(\left|S_{11}\right|^2 + \left|S_{31}\right|^2\right)\right)\left(1 - \left(\left|S_{31}\right|^2 + \left|S_{13}\right|^2\right)\right)}. \quad (2)$$

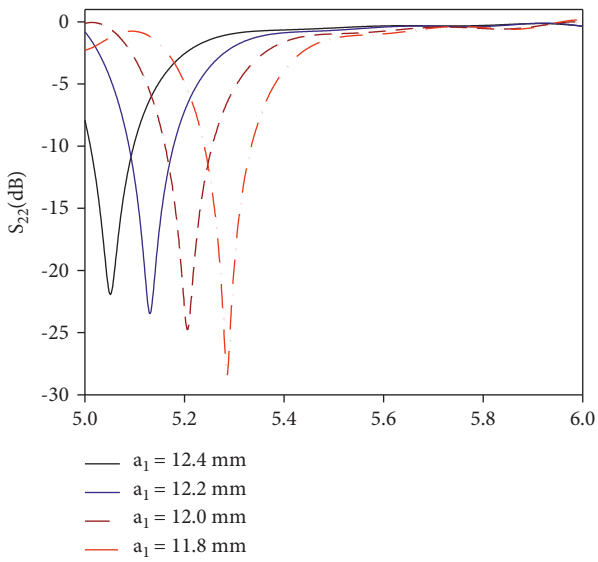

Figure 7: S_{11} against frequency with different lengths of Cav_1.

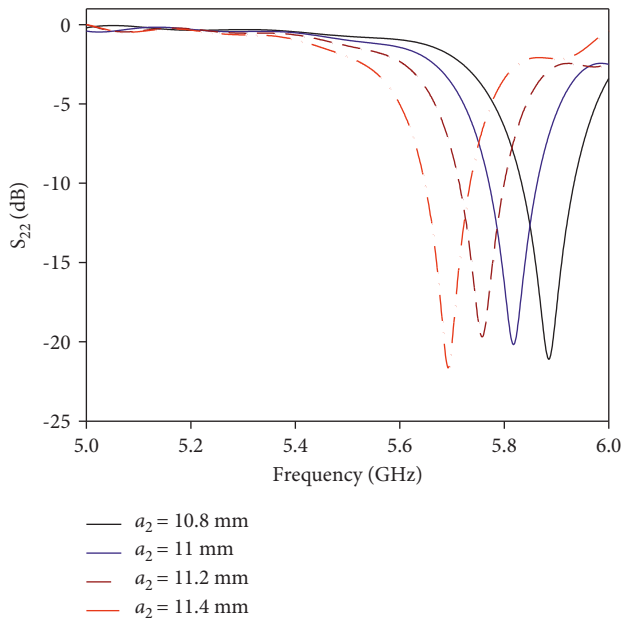

Figure 8: S_{22} against frequency with different lengths of Cav_2.

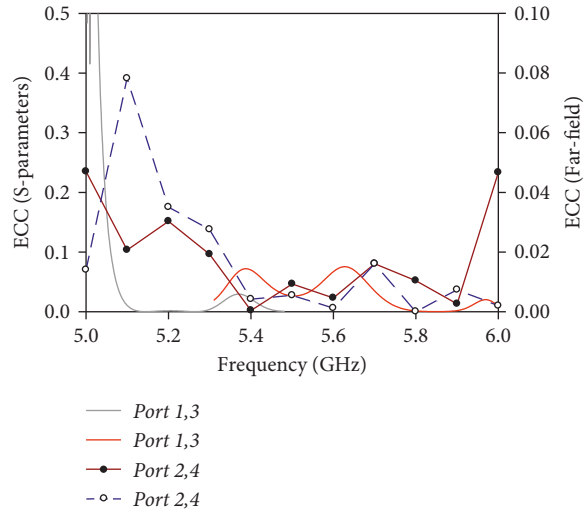

Figure 9: ECC-graphs against frequency from *S*-parameters and far field.

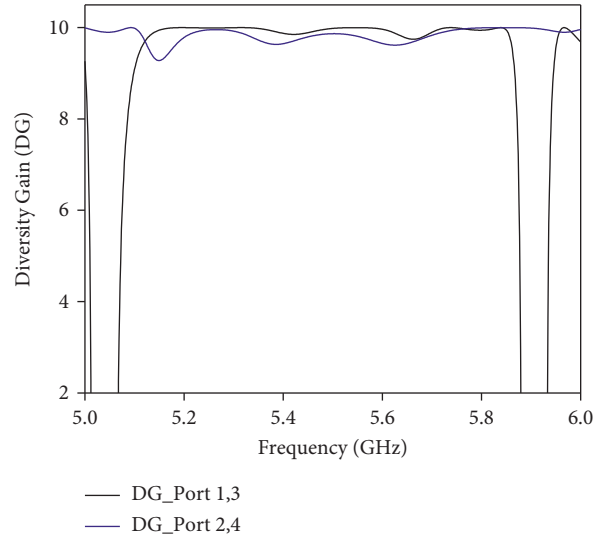

Figure 10: DG against frequency when same cavities are fed simultaneously.

Similarly, the ECC in the upper-frequency band can be evaluated using (2) just by replacing *Port 1* with *Port 2* and *Port 3* with *Port 4*. The ECC values from far-field gain are evaluated and displayed in Figure 9. It shows the peak value in the lower frequency band is around 0.08, while in the upper-frequency band it is around 0.18.

The diversity gain (DG) signifies a rise in the antenna gain with the addition of multiple elements [9]. The DG values are evaluated and presented in Figure 10. After inserting the other cavities, the DG value of the MIMO antenna approaches around 9.94 dB, which approaches its typical value of 10, and it can be obtained by (3) [19].

$$DG = 10\sqrt{1 - |0.99\,Ecc|^2}. \quad (3)$$

2.2. Design Steps. The design guidelines for the proposed MIMO systems are as follows:

(a) Design a square cavity resonator (SIW).

(b) Split the FMSIW cavity into two equal parts along the central magnetic wall.

(c) Insert an open-ended slanted rectangular slot in the HMSIW cavity to convert into two unequal QMSIW cavity resonators (Cav_1 and Cav_2).

(d) Excite each cavity with a microstrip feed line and optimize the dimensions of Cav_1 and Cav_2 to achieve

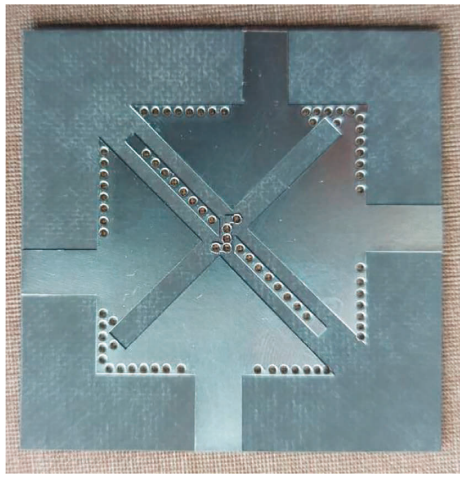

Figure 11: Fabricated prototype of 2 × 2 MIMO antenna-diplexer.

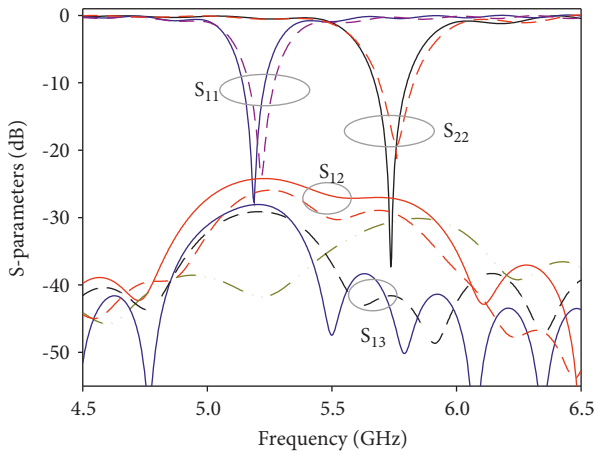

Figure 12: Simulated and measured *S*-parameters against frequency response (solid curve represents simulated graph and dashed curve signify the measured responses).

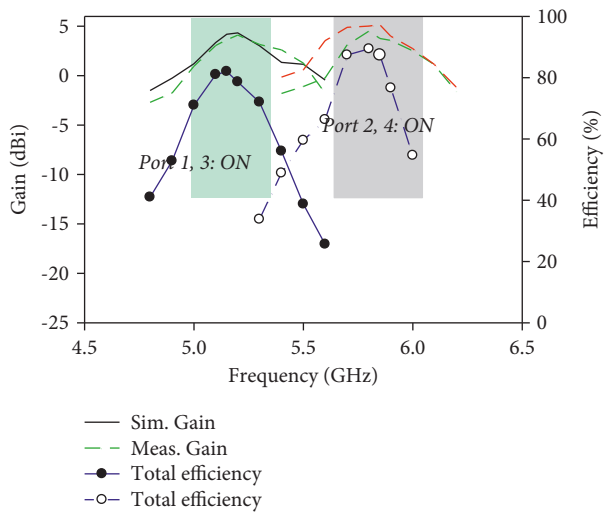

Figure 13: Simulated and measured gain and efficiency against frequency.

the fundamental mode around 5.2 GHz and 5.8 GHz, respectively.

(e) Replicate the 2-elements in the diplexing antenna to achieve a 2 × 2 MIMO antenna.

(f) Optimise the isolation of the relevant dimensions. Evaluate the MIMO performance.

3. Results-Validation and Discussions

A prototype of the proposed dual-band self-diplexing 2 × 2 MIMO antenna system is fabricated using a Rogers-5880 copper laminated dielectric substrate, as shown in Figure 11. The dielectric substrate has a thickness of 1.578 mm and a relative permittivity of 2.2. The simulated scattering parameter responses have been revealed in Figure 12. The operating frequency bands show the port isolation as better than −25 dB. The measurements are performed using the E5080A VNA. The antenna generates resonant frequencies from simulations at 5.2 GHz when *Port-1* or *Port-3* is fed, and *Port-2*/*Port-4* is terminated with matched loads, while it yields resonant frequencies at 5.2 GHz when *Port-2* or *Port-4* is fed, and *Port-1*/*Port-3* is matched terminated. On the other hand, the antenna shows the measured results at 5.25 and 5.84 GHz when the corresponding port is excited, respectively. The antenna generates the peak simulated values of gain of 4.75 and 4.9 dBi and measured values of gain of 4.7 and 4.67 dBi in the lower and upper-frequency bands, respectively. Also, the antenna demonstrates a flat response of the gain curve in both operating frequency bands as the quarter fundamental mode is used for the operation. The radiation efficiency varies in the range of 78%~82% in the frequency band of 5.1~5.35 GHz, while it varies 81%~87% in the upper-frequency band of 5.7~5.89 GHz, as shown in Figure 13. The simulated results closely follow the measured results.

However, a slight difference is witnessed due to the shared coupling of fields generated by the adjoining elements. However, the impact of field coupling on antenna performance is minor. The 2D-radiation patterns of the antenna are plotted at two planes ($\phi = 0^{o}$) and ($\phi = 90^{o}$) in Figure 14. The simulated and measured 2D radiation patterns are plotted at 5.2 GHz in the lower frequency band and at 5.8 GHz in the upper-frequency band. The co/cross-polarization ratio is better than 18 dB in the lower frequency band, while 16 dB is in the higher frequency bands. The proposed design contributes primarily to radiation unidirectional with a front-to-back ratio of better than 18 dB for both operating frequency bands. Additionally, the antenna radiates highest in the broadside direction and has a unidirectional radiation pattern at each resonance due to the involvement of the SIW-backed cavity with the complete ground plane. The proposed MIMO antenna is remarkably compliant in adjusting the resonant frequency in the desired frequency bands. The operating bands can be shifted on either side of the resonant dip individually without affecting performance merely by modifying the dimensions of the QMSIW cavities. The design of the proposed antenna is straightforward, low-profile, small, and easily tunable. The

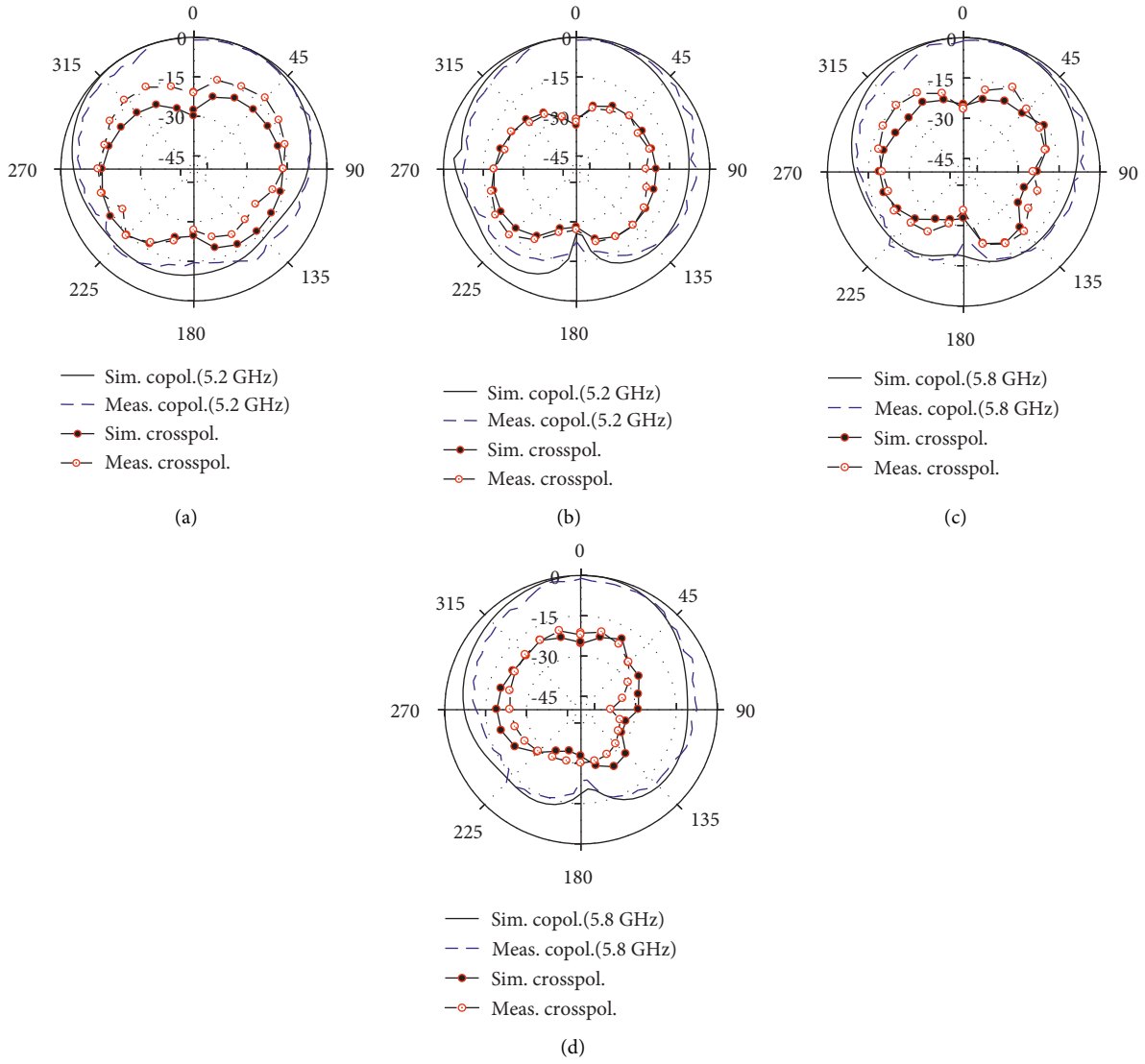

Figure 14: Simulated and measured radiation patterns at 5.2 GHz. (a) E-plane ($\phi = 0^{o}$), (b) H-plane ($\phi = 90^{\circ}$), and 2D radiation patterns at 5.8 GHz, (c) E-plane ad (d) H-plane.

Table 2: Comparison of proposed mimo antenna with other existing works.

Ref	MIMO elements	fr (GHz)	Gain (dBi)	Fractional bandwidth	Isolation (dB)	Size in (electrical length)
[4]	2 × 2	2.5	2.6	2	28	2.5 $\lambda_1 \times 2.5\ \lambda_1$
[16]	2 × 2	3.27 5.4	4.8 5.3	6.6 2.6	20	1.42 $\lambda_1 \times 1.42\ \lambda_1$
[17]	2 × 2	3.5 5.2	2.7 2.8	1.7 1.2	18.4	0.65 $\lambda_1 \times 0.65\ \lambda_1$
[18]	2 × 2	4.43 5.39	6 6.4	2.5 1.8	35	1.7 $\lambda_1 \times 0.8\ \lambda_1$
[20]	2 × 2	2.93 5.68	4 4	35 6.86	14	0.8 $\lambda_1 \times 0.8\ \lambda_1$
[21]	2 × 2	3.51	4.9	≈ 2.7	14	0.35 $\lambda_1 \times 0.86\ \lambda_1$
This work	2 × 2	5.2 5.8	4.85 4.6	1.8 2.2	25	0.7 $\lambda_1 \times 0.7\ \lambda_1$

proposed design is an efficient alternative to enhance the data speed by offering spatial diversity/spatial multiplexing for WLAN communication.

The novel features of the proposed 4-element MIMO antenna are associated with other similar research works, summarized in Table 2. The dual-band self-diplexing antenna shows compact size, better isolation, and comparable gain.

Profile with other similar works. The antennas presented in [16, 20, and 21] show better fractional bandwidth; however, the isolation level is poor. The antennas present similar gain and bandwidth features to [17, 18], and [21] in a more compact design. The port decoupling is better than many other works without using the defected ground structure (DGS) element in the ground plane, which makes this design configuration simple and unique.

4. Conclusion

This paper represents a simple and compact quarter-mode SIW cavity-backed MIMO antenna for two-channel frequency applications. By employing the quarter-mode cavity, the overall size of the proposed structure is miniaturized by around 75% compared to the full-mode cavity. The dual-band operations are achieved by employing two-QMSIW cavities of different dimensions. Later, the cavities are replicated with two more cavities to achieve a MIMO antenna system. To improve the intrinsic isolation levels between any two radiating portions, parasitic metallic strips loaded with shorting vias are placed between two similar cavities. The diversity features are evaluated in terms of ECC and DG; both parameters satisfy the requirements of MIMO communication. The proposed MIMO antenna design is fabricated and practically validated. The measured and simulation show good mutual agreement with each other.

Data Availability

The data used to support the findings of this study are included within the article.

Conflicts of Interest

The authors declare that they have no conflicts of interest.

Acknowledgments

The authors would like to thank the Rogers Corporation (USA) for providing sample substrates.

References

[1] T. Sreenath Reddy, "Rajkishor kumar, and raghvendra kumar chaudhary, "isolation enhancement and radar cross section reduction of MIMO antenna with frequency selective surface," *IEEE Transactions on Antennas and Propagation*, vol. 66, no. 3, pp. 1595–1600, 2018.

[2] I. Rosaline, A. Kumar, P. Upadhyay, and A. H. Murshed, "Four element MIMO antenna systems with decoupling lines for high-speed 5G wireless data communication," *International Journal of Antennas and Propagation*, vol. 25, pp. 1–13, 2022.

[3] A. J. Alazemi and A. Iqbal, "A high data rate implantable MIMO antenna for deep implanted biomedical devices," *IEEE Transactions on Antennas and Propagation*, vol. 70, no. 2, pp. 998–1007, 2022.

[4] A. Boukarkar, X. Q. Lin, Y. Jiang, L. Y. Nie, P. Mei, and Y. Q. Yu, "A miniaturized extremely close-spaced four-element dual-band MIMO antenna system with polarization and pattern diversity," *IEEE Antennas and Wireless Propagation Letters*, vol. 17, no. 1, pp. 134–137, 2018.

[5] Y. Hao and C. G. Paini, "Isolation enhancement of anisotropic UC-PBG microstrip diplexer patch antenna," *IEEE Antennas and Wireless Propagation Letters*, vol. 1, pp. 135–137, 2002.

[6] G. Zhai, Z. N. Chen, and X. Qing, "Enhanced isolation of a closely spaced four-element MIMO antenna system using metamaterial mushroom," *IEEE Transactions on Antennas and Propagation*, vol. 63, no. 8, pp. 3362–3370, 2015.

[7] S. Wang and Z. Du, "Decoupled dual-antenna system using crossed neutralization lines for LTE/WWAN smartphone applications," *IEEE Antennas and Wireless Propagation Letters*, vol. 14, pp. 523–526, 2015.

[8] J. Deng, J. Li, L. Zhao, and L. Guo, "A dual-band inverted-F MIMO antenna with enhanced isolation for WLAN applications," *IEEE Antennas and Wireless Propagation Letters*, vol. 16, pp. 2270–2273, 2017.

[9] P. Cheong, K.-F. Chang, W.-W. Choi, and K.-W. Tam, "A highly integrated antenna-triplexer with simultaneous three-port isolations based onmulti-mode excitation," *IEEE Transactions on Antennas and Propagation*, vol. 63, no. 1, pp. 363–368, Jan. 2015.

[10] K. Dhwaj, X. Li, L. J. Jiang, and T. Itoh, "Low-profile diplexing filter/antenna based on common radiating cavity with quasielliptic response," *IEEE Antennas and Wireless Propagation Letters*, vol. 17, no. 10, pp. 1783–1787, 2018.

[11] A. Kumar, D. Chaturvedi, and S. I. Rosaline, "Design of antenna multiplexer for seamless on-body internet of medical things (IoMT) connectivity," *IEEE Transactions on Circuits and Systems II: Express Briefs*, vol. 69, no. 8, pp. 3395–3399, 2022.

[12] A. Kumar and A. A. Althuwayb, "SIW resonator-based duplex filtenna," *IEEE Antennas and Wireless Propagation Letters*, vol. 20, no. 12, pp. 2544–2548, 2021.

[13] S. Sharma, P. Nigam, A. Muduli, and A. Pal, "Highly isolated self-multiplexing 5G antenna for IoT applications," in *Blockchain for 5G-Enabled IoT*, pp. 593–619, Springer Int, Cham, Switzerland, 2021.

[14] A. Iqbal, I. B. Mabrouk, M. Al-Hasan, M. Nedil, and T. A. Denidni, "Wideband substrate integrated Waveguide antenna for full-duplex systems," *IEEE Antennas and Wireless Propagation Letters*, vol. 21, no. 1, pp. 212–216, 2022.

[15] A. Kumar, D. Chaturvedi, and S. Raghavan, "Design of a self-diplexing antenna using SIW technique with high isolation," *AEU-International Journal of Electronics and Communications*, vol. 94, pp. 386–391, 2018.

[16] B. Niu and J. H. Tan, "Compact two-element MIMO antenna based on half-mode," *Progress In Electromagnetics Research Letters*, vol. 85, pp. 145–149D, 2019.

[17] D. Sarkar and K. V. Srivastava, "Compact four-element SRR loaded dual-band MIMO antenna for WLAN/WiMAX/WiFi/4G-LTE and 5G applications," *Electronics Letters*, vol. 53, no. 25, pp. 1623-1624, 2017.

[18] A. A. Elobied, X. X. Yang, N. Xie, and S. Gao, "dual-band 2× 2 MIMO antenna with compact size and high isolation based on

half-mode SIW," *International Journal of Antennas and Propagation*, vol. 2020, Article ID 2965767, 2020.

[19] B. Pramodini, D. Chaturvedi, and G. Rana, "Design and investigation of dual-band 2 × 2 elements MIMO antenna-diplexer based on half-mode SIW," *IEEE Access*, vol. 10, pp. 79272–79280, 2022.

[20] A. Sharma, A. Sarkar, A. Biswas, and M. J. Akhtar, "Dual-band multiple-input multiple-output antenna based on half split cylindrical dielectric resonator," *Journal of Electromagnetic Waves and Applications*, vol. 32, no. 9, pp. 1152–1163, 2018.

[21] B. Niu and J. H. Tan, *Progress In Electromagnetics Research Letters*, vol. 88, pp. 143–149, 2020.

[22] A. Kumar, D. Chaturvedi, M. Saravanakumar, and S. Raghavan, "SIW cavity-backed self-triplexing antenna with T-shaped slot," in *Proceedings of the Asia-Pacific Microwave Conference (APMC)*, pp. 1588–1590, IEEE, Kyoto, Japan, November 2018.

[23] T. Sreenath Reddy, "Rajkishor kumar, and raghvendra kumar chaudhary, "isolation and frequency reconfigurable compact MIMO antenna for WLAN applications" IET Microwave," *Antenna and Propagation (IET MAP)*, vol. 13, no. 4, pp. 519–525, 2019.

[24] A. Kumar, D. Chaturvedi, and S. Raghavan, "Dual-band, dual-fed self-diplexing antenna," in *Proceedings of the 13th European Conference on Antennas and Propagation (EuCAP)*, pp. 1–5, IEEE, Krakow, Poland, March 2019.

[25] A. Iqbal, M. Al-Hasan, I. B. Mabrouk, and M. Nedil, "A compact implantable MIMO antenna for high-data-rate bio-telemetry applications," *IEEE Transactions on Antennas and Propagation*, vol. 70, no. 1, pp. 631–640, Jan. 2022.

Hindawi
International Journal of Antennas and Propagation
Volume 2022, Article ID 5964753, 9 pages
https://doi.org/10.1155/2022/5964753

Research Article

Design of Wideband Circular-Slot Antenna for Harvesting RF Energy

Surajo Muhammad,[1] **Amor Smida**,[2] **Mohamed Ibrahim Waly**,[2] **Nazih Khaddaj Mallat**,[3] **Amjad Iqbal**,[4] **Sadeque Reza Khan**,[5] **and Mohammad Alibakhshikenari**[6]

[1]*Department of Electronics and Telecommunication Engineering, Ahmdu Bello University, Zaria 810211, Nigeria*
[2]*Department of Medical Equipment Technology, College of Applied Medical Sciences, Majmaah University, AlMajmaah 11952, Saudi Arabia*
[3]*College of Engineering, Al Ain University, Al Ain 64141, UAE*
[4]*Institut National de la Recherche Scientifique (INRS), Montréal H5A 1K6, QC, Canada*
[5]*Institute of Integrated Micro and Nano Systems, School of Engineering, University of Edinburgh, Edinburgh EH9 3FF, UK*
[6]*Department of Signal Theory and Communications, Universidad Carlos III de Madrid, Leganés 28911, Madrid, Spain*

Correspondence should be addressed to Mohammad Alibakhshikenari; mohammad.alibakhshikenari@uc3m.es

Received 2 June 2022; Accepted 30 June 2022; Published 19 July 2022

Academic Editor: Arvind Kumar

The design of a wideband circular-slot antenna for RF signal harvesting is reported in this work. The proposed design frequency range accommodates the leading contributors to the available RF signals accessible by the RFEH node. These widely utilized frequency bands comprise GSM1800, UMTS2100, Wi-Fi2.450, and LTE2600. The antenna geometry comprises circular-ring radiating component filled with two orbital circular and rectangular slots. At the bottom plane, a pair of rectangular and semirectangular-circle slits are integrated. The antenna presented is designed on a double layer of 1.6 mm high FR-4 substrate. The source antenna achieved a simulated and measured impedance bandwidth (BW) of 1.510 and 1.590 GHz, amounting to 68% and 73% fractional BW (FBW), covering -10 dB reflection coefficient ($|S_{11}|$) between 1.640 to 3.150 GHz and 1.550 to 3.140 GHz, in that order. The wideband circular-slot source antenna realized a maximum measured gain of 1.88, 2.13, 2.81, 3.22, and 4.32 dBi for 1.800, 2.100, 2.450, 2.650, and 3.20 GHz, respectively. The proposed design dimension on the printed board is 0.61 $\lambda_g \times 0.70\ \lambda_g$. The improved antenna gain is obtained from a circular parasitic patch coupled to the defected ground structure (DGS) for better RF energy harvesting in an ambient environment.

1. Introduction

The ability to handle high electromagnetic (EM) energy is one of the important features of antennae used for the RFEH module [1, 2]. RFEH technology has recently piqued the interest of researchers as an additional source of energy that provides an alternative solution to short-life batteries [3, 4]. Mobiles phones and other related wireless devices have been penetrating the market since 1980 [1, 5]. Hence, the rising demand for the long operational life of a battery remains an open challenge [6, 7]. In RFEH systems, a rectifying antenna (rectenna) harvests the energy via a combination of a source antenna and RF-rectifier [8, 9]. The source antenna picks up the incoming signals, which are then transformed by an RF-rectifier into a useable low power dc supply [10]. RFEH technology is considered among the sources of green energy by utilizing and shielding humanity from potentially harmful radiation [11]. Thus, wireless medical implanted devices (WMID) largely facilitated the emergence of applications in healthcare systems such as wirelessly capsule endoscopes, neural implants, retinal prostheses, various neural recording microsystems, spinal cord stimulators, and

intracranial pressure (ICP) monitors [12, 13]. Life-saving healthcare systems involve telemetry and supervision of the vital human body parts by the basic essential indicators for the evaluation, diagnosis, stimulation, and treatment process [14, 15]. RFEH antennae with wide operational BW and improved gain are desirable for an efficient RF harvester [16]. RF-spectral data from various research studies that have recently been reported shows a practical amount of energy for harvesting at GSM1800, UMTS2100, ISM2.4-Wi-Fi2.45, and LTE2600 spectrum [5]. It is a challenging task to design an antenna that can operate over a specific broad and compact spectrum for a particular application [17, 18].

Researchers have recently focused on developing ultra-wideband antennae with band rejection capabilities to minimize interference from narrow-band for wireless applications [19, 20]. To attain the desired goal, several designs approach, such as inserting slits and slots of varying diameters, are being applied to the radiating components, feed line, and ground planes [5, 19]. The use of half ($\lambda/2$) [5] and a quarter ($\lambda/4$) [21] wavelength, open ended slits, and DGS [22, 23] are also reported for various wireless communications applications. The authors in [24] introduce a circular patch monopole antenna with an annular-ring structure at 5.80 GHz. The antenna demonstrates a 12.8% BW increment, and a gain of 5.70 dBi at a relatively high frequency compares to a typical monopole antenna. A monopolar broadband antenna is reported by the authors in [25]. With the introduction of metallic Vias, the antenna attains a BW of 18%, resulting in a peak realized gain of 6 dBi between 2.15 and 2.35 GHz.

Incorporating a feeding-loop results in about 65% BW as demonstrated by the authors in [26]. The antenna realized a peak gain in the span of 3 to 7.7 dBi between 1.320 and 2.60 GHz operating frequencies (f_o). Besides, the deployment of a complex feeding technique in the 3D structural model, a CPW broadband antenna with a square-slotted pattern is demonstrated by the authors in [27]. The design realized a FBW of 17.2% at 2.440 GHz. The concept of introducing slots and slits on the feed line and the bottom ground of the CPW antenna is reported to improve the FBW by about 45% by the authors in [28, 29]. The authors in [30] explore the analysis of corner truncated antennae comprising U and L slots. A single feed probe is used in the design study where the various dimensions of the substrate height (h) were examined. The design attained a peak FBW of 14.0% at 4.05 and 4.15 GHz. The authors [31, 32] demonstrated the concept of integrating the feed line with slots and slits. The designs, respectively, realized a FBW of 4.70% and 17.70% for worldwide interoperability for microwave access (WiMax) and radio frequency identification (RFID) applications. The technique of fractal architectures deployed by the authors in [33–35] obtained a FBW of 22.50%, 0.78%, and 2.00%, respectively. Hence, the broadband antennae reported by the authors in [28, 29, 31] and [36] are generally designed with a complicated geometry that is difficult to actualize.

This work targets a wideband circular-slot antenna with an improved gain, having a simple and inexpensive geometry structure. The authors in [34, 37] demonstrated the concept of an electromagnetic coupling using a single feed line to maintain simple antenna geometry. A tilted rectangular and triangular wideband monopole printed antennae are exploited by the authors in [38, 39]. The designs reported a FBW of 51.40% and 62.00%, respectively. The designs also recorded a relatively low gain across the f_o, which renders them unsuitable for low-power RFEH systems. A low-profile source antenna with broad BW and enhanced gain is required for better RFEH in ambient terrain [1, 10]. A broadband antenna for RFEH is presented by the authors in [40]. The antenna achieved a FBW of 23% at 2.45 GHz. The authors in [41] reported a narrow-band antenna for the RFEH application. The source antenna achieved a 10 dB BW of 30 MHz with a peak gain of 3.360 dBi at 2.45 GHz. Printed patch antennae are regaining recognition in the design of RF harvesters due to their conformability to planar and nonplanar surfaces, compactness, low-profile, light, and cheap manufacturing cost [1, 8, 11]. Patch antennae are also preferred due to their adaptability in terms of f_o, gain, radiation pattern, polarization, and matching BW. Therefore, the proposed design in this work maintains a trade-off between simple geometry structures, compact size, affordability, and improve performance.

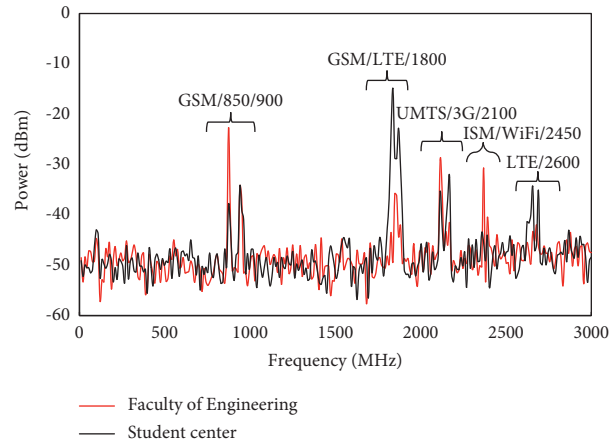

Figure 1: Evaluation of the received RF ambient power levels.

In this study, a circular-slot wideband antenna is reported. The antenna is suitable for harvesting RF signals across GSM1800, UMTS2100, ISM2.4-Wi-Fi2.45, and LTE2600 spectrum. The proposed design achieved a total dimension of 50 mm × 56 mm matched through a 50 Ω transmission line (TL). The proposed design offers a wide f_o of 1.640 GHz to 3.150 GHz with an improved gain applicable for RFEH systems. The remaining sections of this work are divided into the following. Section 2 outlines the proposed design antenna configuration. The findings are addressed in Section 3. The concluding remark is presented in Section 4.

2. Antenna Design

RF spectrum measurements were performed before coming out with the antenna design to determine the availability of RF ambient power in the environment. Figure 1 presents a

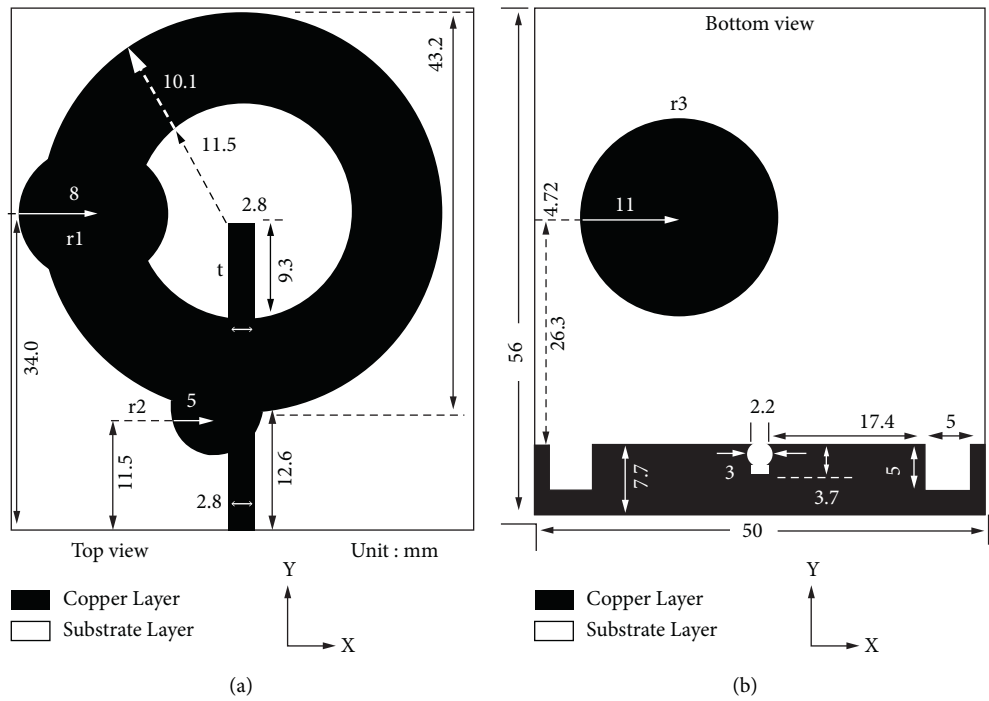

Figure 2: Proposed wideband antenna design architecture: (a) top view and (b) bottom view.

cross section of the received ambient RF power levels. The survey highlights the significance of five major spectrums with reasonable power levels for RFEH. As a result, the operational frequency for the proposed antenna is specified within 1.640 to 3.150 GHz, which covers GSM1800, UMTS2100, ISM2.4Wi-Fi2.45, and LTE2600 frequency bands.

The antenna presented in this paper is designed on a double layer of 1.6 mm height (h) FR-4 substrates, having 4.7 dielectric constant (ϵ_r), with 0.02 tangent loss (tanδ). The material is adopted because it is inexpensive, available, and simple to fabricate. The proposed antenna comprises a circular-ring radiating element integrated with two additional circular and rectangular slots. Figure 2 presents design architecture and the parameters of the proposed wideband circular-slot antenna. Firstly, antenna architecture was a model using a circular microstrip planar antenna based on a closed-form equation as expressed in the following equation [42]:

$$f_{\mathrm{lw}} = 7.2\left\{\frac{9a + 4p}{4} \times k\right\}^{-1} GHz, \tag{1}$$

where f_{lw} represents the lower cutoff f_o. p is the gap of the feed line in (cm). a provides the radius of the circular patch in (cm) over a constant value $k = 1.15$. Thus, "a" can be expressed as

$$a = \left\{\frac{3.20\,(GHz)}{f_{lw} \times \kappa}\right\} - \left\{\frac{4}{9}\right\} p. \tag{2}$$

Solving for "a" at $f_{lw} = 1.6$ GHz, and $p = 0.5$ cm, a is computed to be 1.6 cm (16 mm). The width of TL is initially evaluated at 2.7 mm from the Wheeler's closed-form equation [10] and then optimized at 2.8 mm. The calculated values from the model equation are transferred into a high-frequency structure simulator (HFSS) from ANSYS for further parametric tuning and optimization.

This section investigates the impact of various critical dimensional elements on the antenna's performance, notably its radiation pattern, impedance BW, and gain. All simulations are conducted through HFSS. The first circular antenna structure (Design-#1) resonates at 2.2 GHz with an unsatisfactory $|S_{11}|$. Circular structures tend to provide a steady flow of currents [15, 33]. A DGS is introduced into the antenna structure to achieve a broader impedance BW between 1.600 and 3.100 GHz as depicted in Design-#2. A circular-ring structure is realized by introducing a 23 mm circular slot into the radiator, as shown in Design-#3. Two circular slots are added to the orbital section of the radiator to achieve a broader resonance across 2.320 to 2.910 GHz f_o. A good impedance matching is realized by extending rectangular slots from the bottom of the radiator. The DGS is also incorporated with a resonating circular parasitic patch to enhance the proposed antenna's gain. The embedded circular patch on the partial ground resonates with the corresponding pair of circular slots counterpart on the left-hand side (LHS) of the radiator. Additionally, a pair of rectangular slots and a semirectangular-circle slit are carved on the bottom ground for a broader impedance BW as described in Design-#4. The addition of the slots and slits into the orbital sides of the structure is realized through considerable parametric analysis to maintain the antenna wideband characteristics with a reasonable gain. Hence, Figure 3 illustrates the procedures used to achieve the desired wideband circular-slot antenna.

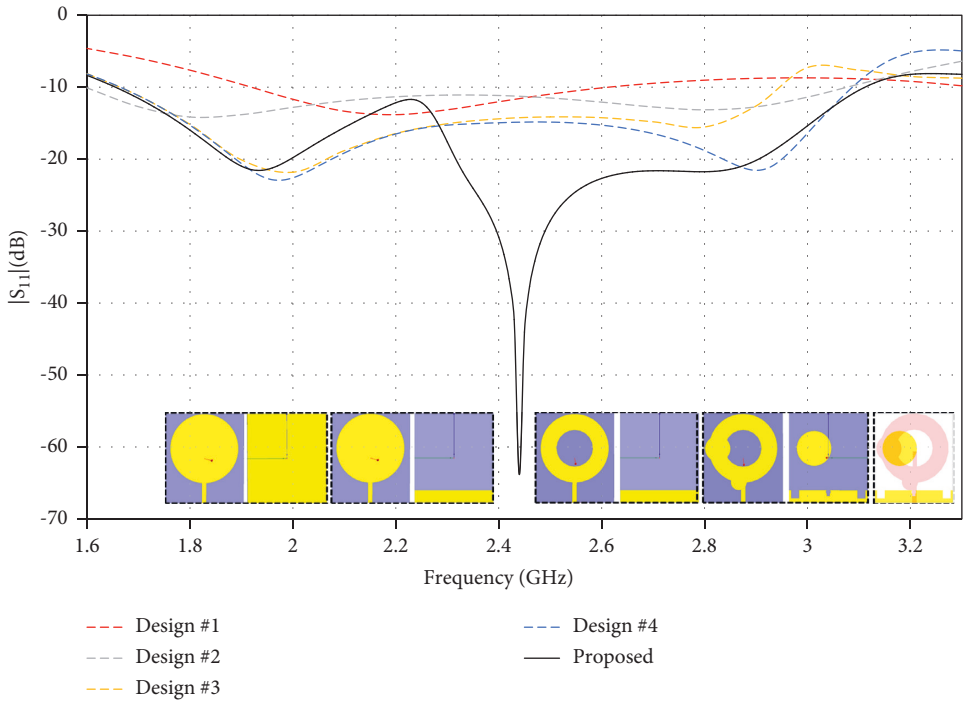

Figure 3: Design approach for optimizing the proposed wideband circular-slot antenna from a basic circular antenna structure.

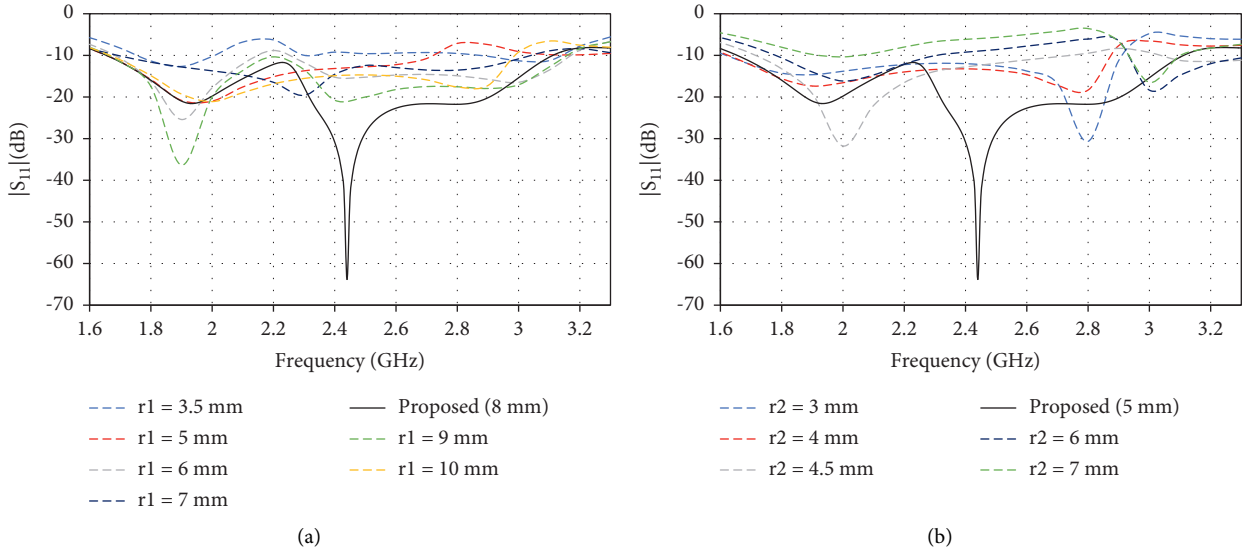

Figure 4: Parametric analysis of the two orbital circular slots. (a) $r1$ and (b) $r2$.

The wideband circular-slot radiator is first excited with an upper circular slot along the LHS corner with a radius of $r1$. The diameter of the slot was tuned at $\lambda/4$ of the medium resonance mode of 2.1 GHz. $r1$ was then varied to investigate the effects of the slots on the antenna performance. Adjusting $r1$ introduces a noticeable impedance mismatched along the 2.00 to 2.400 GHz f_o. The diameter of the slots was then optimized at 16 mm, as shown in Figure 4(a). The lower circular slot with a radius of $r2$ is integrated between the radiator and the feed line to further improve the upper resonance mode f_u between 2.320 and 2.910 GHz and also reduce the impedance mismatch. The diameter of the lower orbital slot were then gradually tuned at $\lambda/8$ of f_u at 2.45 GHz. Hence, $r2$ of the slot demonstrates an improved antenna performance at 10 mm diameter, as shown in Figure 4(b).

The incorporation of the upper and lower circular slots to the radiator introduces an impedance mismatch to f_{lw}. As such, a vertical rectangular slot is raised from the center of the radiator to enhance the impedance matching across the wide f_o. Rectangular stubs have been frequently employed in various literature to increase the resonance performance depending on their orientation [43–46]. Varying the length of the slot t has an impact on the impedance BW, which

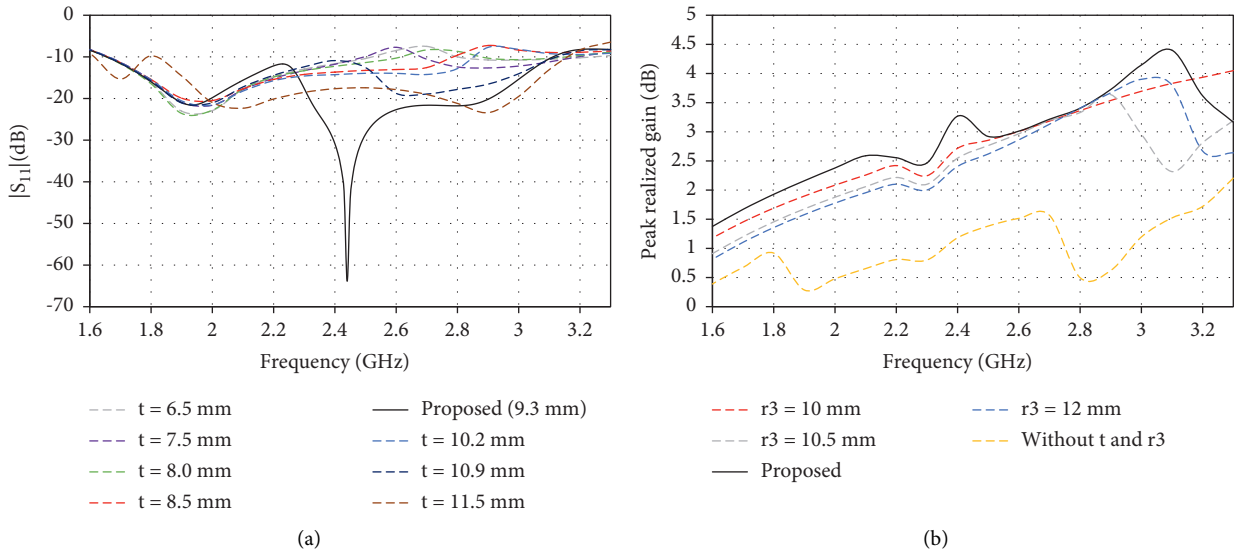

FIGURE 5: (a) Parametric analysis of the centered rectangular slot t and (b) influence of t and $r3$ on gain.

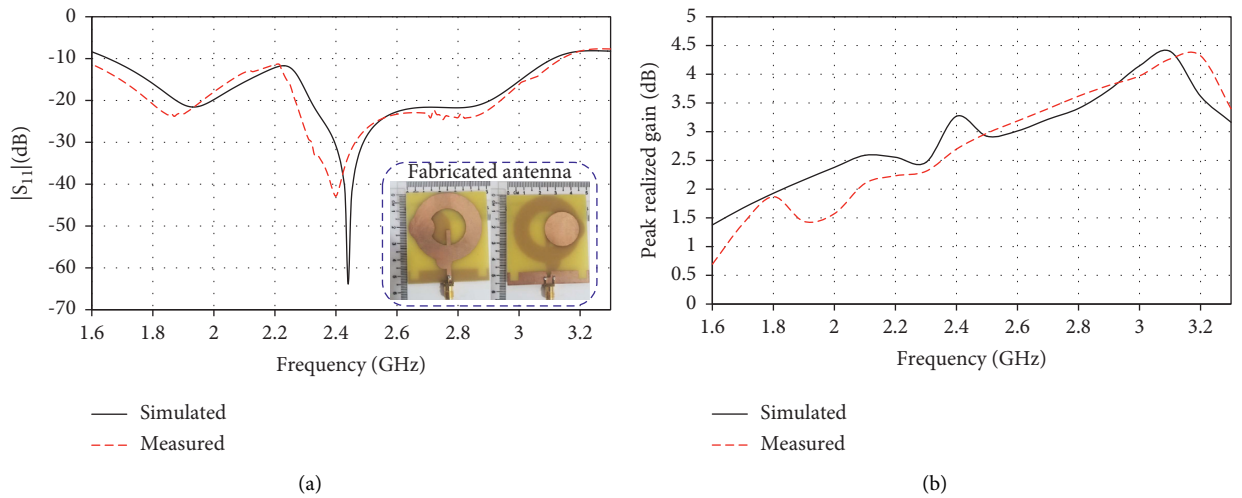

FIGURE 6: Simulated and measured (a) reflection coefficient ($|(S)_{11}|$) and (b) peak realized gain of the proposed wideband circular-slot antenna against frequency.

distorts the antenna peak achievable gain. The impedance matching tends to improve as t slowly increases from 6.5 to 9 mm and deteriorates beyond 10 mm. A good impedance matching is realized by extending the length t of the rectangular slot from the bottom of the radiator at 9.30 mm, as demonstrated in Figure 5(a). Additionally, a circular parasitic patch is embedded into the partial ground to resonate with their corresponding pair of the radiator orbital circular slot to enhance the proposed antenna's gain. A comparison of the circular parasitic patch with radius $r3$ and the corresponding length t is illustrated in Figures 5(a) and 5(b).

3. Results and Discussion

Figure 6(a) presents the results of the simulated and measured $|S_{11}|$ versus the frequency of the proposed wideband circular-slot antenna. The antenna's measured $|S_{11}|$ is in close agreement with the simulated data. The slight variation from the measured data is attributed to fabrication tolerance between the top and bottom view, the SMA source or connection loss, and soldering lead loss. The proposed design achieved -10 dB simulated and measured BW of 1.51 GHz over a frequency span of 1.640 to 3.150 GHz and 1.590 GHz between 1.550 and 3.140 GHz. The results findings cover a target f_o, amounting to 68% and 73% of the simulated and measured FBW, respectively.

Figure 6(b) depicts the peak gain variation as a function of frequency. A maximum peak measured and simulated realized gain of 3.1 dBi and 3.2 dBi is attained by the antenna at 2.600 GHz over a range of the targeted f_o. A peak realized simulated and measured gain of (1.93 dBi, 2.6 dBi, and 3.3 dBi) and (1.8 dBi, 2.1 dBi, and 2.7 dBi) is also achieved at 1.800, 2.100, and 2.400 GHz, respectively.

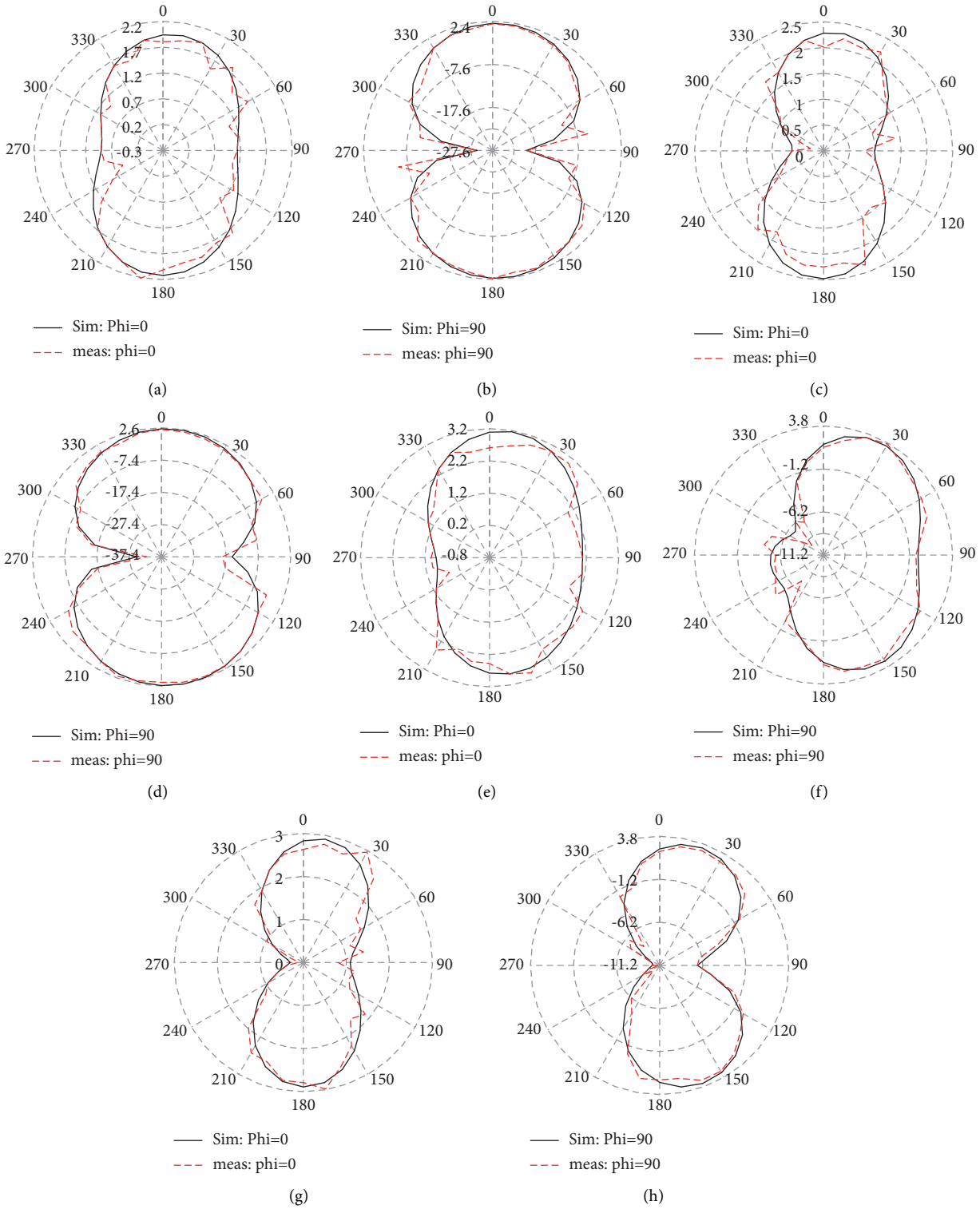

FIGURE 7: Simulated and measured radiation pattern of the proposed wideband circular-slot antenna for Phi = 0^o and Phi = 90^o: (a, b) at 1.8 GHz, (c, d) at 2.1 GHz, (e, f) at 2.45 GHz, and (g, h) at 2.65 GHz, respectively.

Figure 7 presents a 2D radiation plot across the four f_o. The results are simulated at 1.800, 2.100, 2.450, and 2.65 GHz, alongside xz-plane for ($\varphi = 0^o \mid 0^o < \theta < 180^\circ$) and yz-plane for ($\varphi = 90^\circ \mid 0^\circ < \theta < 180^\circ$), respectively. An almost omnidirectional radiation pattern is seen along xz-plane, whereas yz-plane portrays a dipole-antenna pattern at 1.800 and 2.100 GHz, and a directional antenna at 2.450 and 2.650 GHz.

Table 1 summarizes the antenna's outcomes, which are compared with the related work in terms of their

Table 1: Comparison of the proposed wideband circular-slot antenna with the related work.

Ref [...]	Electrical Length (λ_g)	Description	Operating frequency (GHz)	FBW (%)	Maximum realized gain (dBi)	Substrate
[18]	1.52×1.52	Coupled slotted-gap with a semicircular slot.	5.150–12.470	78	4.5	FR-4 (4.3)
[24]	2.70×1.70	Coupled annular ring with a centralized feed point.	5.700–6.300	10	5.7	RO6002 (2.94)
[28]	0.70×0.71	Quasi C-shaped with a centralized signal strip	5.150–7.100	31	3.6	RO4003 (3.55)
[37]	1.10×1.10	Electromagnetically coupled fed a circular pattern	2.410–2.500	3.6	NA	FR-4 (4.5)
[38]	0.95×0.95	Slanted rectangular slots pattern	1.820–3.080	51	1.5	FR-4 (4.7)
[33]	0.80×1.10	Triangular ground with an asymmetrical excitation	1.42–2.7	62	2.2	FR-4 (4.3)
[33]	0.63×0.63	Single fed fractal pattern integrated diagonally with a ring slot	1.370–1.770	25	4.1	FR-4 (4.4)
This work	0.61×0.700	Circular slot with a pair of orbital circular and extended rectangular slots pattern	1.55–3.14	73	4.32	FR-4 (4.7)

*λ_g: guided wavelength at the lowest operating frequency (f_o). NA: not available.

Figure 8: Ambiance measurement setups of the proposed rectenna.

description, electrical dimensions, FBW, and gain. The authors in [18, 24] realized a peak gain when compared to this work at the expense of a larger electrical dimension, lower FBW, and relatively higher f_o. Besides, the proposed wideband circular-slot antenna demonstrates a good improvement with a broader f_o that covers four major RFEH spectrums. Furthermore, the antenna achieved a high gain across f_o, which is important in energy harvesting applications. As a result, the antenna provides a good trade-off between FBW, compact size, gain, and cost.

The performance of the proposed wideband circular-slot antenna in an ambiance terrain is investigated in the Multimedia University, Cyberjaya campus. Figure 1 highlights the capability of the terrain for harvesting RF signals. The amplitudes of receiving RF signals vary based on the ambient circumstances. After evaluating the antenna parameters, a broadband RF-rectifier with a wide scale of input power is introduced to make a rectenna system. The RF-rectifier also operates between 1.780 and 2.620 GHz. The two components are connected by a straight-through SMA-male to a SMA-male RF adapter. The broadband rectenna is then put to the test in an ambiance setting. The proposed wideband circular-slot antenna is subjected to a variety of tests at different locations in the campus through the rectenna system. Generally, the locations are marked between 30 and 200 meters from a nearby position or BS. The measurements location is around 1 to 2 m above the surface level. As demonstrated in Figure 8, the proposed circular-slot antenna produces an output dc voltage V_{dc} of 0.313 V via the wideband RF-rectifier output terminal.

4. Conclusion

Source antenna architecture presented in this paper is composed of a circular-ring radiating element loaded with two orbital circular and rectangular slots. A defected ground integrated with a pair of rectangular and semirectangular-circle slits is modeled at the bottom plane for enhancing the impedance matching BW. A circular parasitic patch resonating with its respective pair of radiator orbital slots is further added into DGS to improve the gain of the proposed antenna. The proposed wideband circular-slot antenna achieved a measured and simulated operational BW of 1.59 and 1.510 GHz, resulting to a 73% and 68% FBW, respectively. A peak measured and simulated realized gain of (1.8 dBi, 2.1 dBi, 2.7 dBi, and 3.1 dBi) and (1.93 dBi, 2.6 dBi, 3.4 dBi, and 3.2 dBi) is attained by the antenna at 1.800, 2.100,

2.450, and 2.650 GHz, in that order. The source antenna is implemented on the FR-4 board covering a size of 0.61 $\lambda_g \times 0.70\ \lambda_g$ [47].

Data Availability

The data used to support the findings of this study are included within the article.

Conflicts of Interest

The authors declare that they have no conflicts of interest.

Acknowledgments

Dr. Mohammad Alibakhshikenari acknowledges support from the CONEX-Plus programme funded by the Universidad Carlos III de Madrid and the European Union's Horizon 2020 research and innovation programme under the Marie Sklodowska-Curie grant agreement no. 801538.

References

[1] I. Adam, M. N. Yasin, P. J. Soh et al., "A simple wideband electromagnetically fed circular polarized antenna for energy harvesting," *Microwave and Optical Technology Letters*, vol. 59, no. 9, pp. 2390–2397, 2017.

[2] S. Muhammad, J. J. Tiang, and S. K. Wong, "Design of a dual-port multi-band rectifier circuit," in *Proceedings of the 8th Global Conference on Engineering and Technology (CIETR - 2020)*, Bangkok, Thailand, December 2020.

[3] B. R. Behera, P. R. Meher, and S. K. Mishra, "Microwave antennas-An intrinsic part of RF energy harvesting systems: a contingent study about its design methodologies and state-of-art technologies in current scenario," *International Journal of RF and Microwave Computer-Aided Engineering*, vol. 30, no. 5, Article ID e22148, 2020.

[4] S. Muhammad, J. J. Tiang, S. K. Wong et al., "Harvesting systems for rf energy: trends, challenges, techniques, and tradeoffs," *Electronics*, vol. 11, no. 6, p. 959, 2022.

[5] S. Muhammad, A. S. Yaro, and I. B. Alhassan, "Wide-band 4g mobile device planar antenna using couple feeding technique," *ATBU Journal of Science, Technology and Education*, vol. 5, no. 4, pp. 107–116, 2018.

[6] C. Song, Y. Huang, J. Zhou et al., "Matching network elimination in broadband rectennas for high-efficiency wireless power transfer and energy harvesting," *IEEE Transactions on Industrial Electronics*, vol. 64, no. 5, pp. 3950–3961, 2017.

[7] Z.-X. Zhang and X. Y. Zhang, "High-efficiency single- and dual-band rectifiers using a complex impedance compression network for wireless power transfer," *IEEE Transactions on Industrial Electronics*, vol. 65, no. 6, pp. 5012–5022, 2018.

[8] D. Surender, T. Khan, F. A. Talukdar, A. De, Y. M. Antar, and A. P. Freundorfer, "Key components of rectenna system: a comprehensive survey," *IETE Journal of Research*, pp. 1–27, 2020.

[9] D. Chaturvedi, A. Kumar, and S. Raghavan, "Wideband HMSIW-based slotted antenna for wireless fidelity application," *IET Microwaves, Antennas & Propagation*, vol. 13, no. 2, pp. 258–262, 2019.

[10] S. Muhammad, J. Jiat Tiang, S. Kin Wong et al., "Compact rectifier circuit design for harvesting gsm/900 ambient energy," *Electronics*, vol. 9, no. 10, p. 1614, 2020.

[11] K. Niotaki, S. Kim, S. Jeong, A. Collado, A. Georgiadis, and M. M. Tentzeris, "A compact dual-band rectenna using slot-loaded dual band folded dipole antenna," *IEEE Antennas and Wireless Propagation Letters*, vol. 12, pp. 1634–1637, 2013.

[12] A. Iqbal, M. Al-Hasan, I. B. Mabrouk, A. Basir, M. Nedil, and H. Yoo, "Biotelemetry and wireless powering of biomedical implants using a rectifier integrated self-diplexing implantable antenna," *IEEE Transactions on Microwave Theory and Techniques*, vol. 69, no. 7, pp. 3438–3451, 2021.

[13] S. Roy, A. N. M. W. Azad, S. Baidya, M. K. Alam, and F. H. Khan, "Powering solutions for biomedical sensors and implants inside the human body: a comprehensive review on energy harvesting units, energy storage, and wireless power transfer techniques," *IEEE Transactions on Power Electronics*, vol. 37, no. 10, pp. 12237–12263, 2022.

[14] A. Basir, I. A. Shah, and H. Yoo, "Sphere-shaped implantable receiver coil for misalignment-resilient wireless power transfer systems for implantable devices," *IEEE Transactions on Antennas and Propagation*, p. 1, 2022.

[15] A. Kumar and S. Raghavan, "A design of miniaturized half-mode siw cavity backed antenna," in *Proceedings of the 2016 IEEE Indian Antenna Week (IAW 2016)*, pp. 4–7, IEEE, Madurai, India, June 2016.

[16] S. Agrawal, M. S. Parihar, and P. N. Kondekar, "Broadband rectenna for radio frequency energy harvesting application," *IETE Journal of Research*, vol. 64, no. 3, pp. 347–353, 2018.

[17] S. Muhammad, A. S. Yaro, I. Ya'u, and A. Abubakar, "Design of single feed dual-band millimeter wave antenna for future 5g wireless applications," *Science World Journal*, vol. 14, no. 1, pp. 84–87, 2019.

[18] M. K. Verma, B. K. Kanaujia, J. P. Saini, and P. Singh, "A compact multi-slots loaded gap coupled CP antenna with DGS for WLAN/WiMAX applications," *International Journal of RF and Microwave Computer-Aided Engineering*, vol. 30, no. 12, Article ID e22431, 2020.

[19] J. Choi, K. Chung, and Y. Roh, "Parametric analysis of a band-rejection antenna for uwb application," *Microwave and Optical Technology Letters*, vol. 47, no. 3, pp. 287–290, 2005.

[20] R. Eshtiaghi, R. Zaker, J. Nouronia, and C. Ghobadi, "UWB semi-elliptical printed monopole antenna with subband rejection filter," *AEU - International Journal of Electronics and Communications*, vol. 64, no. 2, pp. 133–141, 2010.

[21] I.-J. Yoon, H. Kim, H. Yoon, Y. Yoon, and Y.-H. Kim, "Ultra-wideband tapered slot antenna with band cutoff characteristic," *Electronics Letters*, vol. 41, no. 11, p. 629, 2005.

[22] S. Soltani, M. Azarmanesh, P. Lotfi, and G. Dadashzadeh, "Two novel very small monopole antennas having frequency band notch function using dgs for uwb application," *AEU - International Journal of Electronics and Communications*, vol. 65, no. 1, pp. 87–94, 2011.

[23] Y. Shi, Y. Fan, Y. Li, L. Yang, and M. Wang, "An efficient broadband slotted rectenna for wireless power transfer at lte band," *IEEE Transactions on Antennas and Propagation*, vol. 67, no. 2, pp. 814–822, 2019.

[24] A. Al-Zoubi, F. Yang, and A. Kishk, "A broadband center-fed circular patch-ring antenna with a monopole like radiation pattern," *IEEE Transactions on Antennas and Propagation*, vol. 57, no. 3, pp. 789–792, 2009.

[25] J. Liu, Q. Xue, H. Wong, H. W. Lai, and Y. Long, "Design and analysis of a low-profile and broadband microstrip monopolar patch antenna," *IEEE Transactions on Antennas and Propagation*, vol. 61, no. 1, pp. 11–18, 2013.

[26] L. Cui, W. Wu, and D.-G. Fang, "Wideband circular patch antenna with conical radiation pattern," *IEEE Antennas and Wireless Propagation Letters*, vol. 14, pp. 458–461, 2015.

[27] K.-M. Chang, R.-J. Lin, I.-C. Deng, J.-B. Chen, K. Q. Xiang, and C. J. Rong, "A novel design of a cpw-fed square slot antenna with broadband circular polarization," *Microwave and Optical Technology Letters*, vol. 48, no. 12, pp. 2456–2459, 2006.

[28] S. Ahdi Rezaeieh, A. Abbosh, and M. A. Antoniades, "Compact cpw-fed planar monopole antenna with wide circular polarization bandwidth," *IEEE Antennas and Wireless Propagation Letters*, vol. 12, pp. 1295–1298, 2013.

[29] L. Zhang, Y.-C. Jiao, Y. Ding, B. Chen, and Z.-B. Weng, "Cpw-fed broadband circularly polarized planar monopole antenna with improved ground-plane structure," *IEEE Transactions on Antennas and Propagation*, vol. 61, no. 9, pp. 4824–4828, 2013.

[30] S. S. Yang, K.-F. Lee, A. A. Kishk, and K.-M. Luk, "Design and study of wideband single feed circularly polarized microstrip antennas," *Progress In Electromagnetics Research*, vol. 80, pp. 45–61, 2008.

[31] J.-Y. Jan, C.-Y. Pan, K.-Y. Chiu, and H.-M. Chen, "Broadband cpw-fed circularly-polarized slot antenna with an open slot," *IEEE Transactions on Antennas and Propagation*, vol. 61, no. 3, pp. 1418–1422, 2013.

[32] J.-H. Wang and S.-F. Wang, "Planar broadband circularly polarized antenna with square slot for uhf rfid reader," *IEEE Transactions on Antennas and Propagation*, vol. 61, no. 1, pp. 45–53, 2013.

[33] J. Kizhekke Pakkathillam and M. Kanagasabai, "Circularly polarized broadband antenna deploying fractal slot geometry," *IEEE Antennas and Wireless Propagation Letters*, vol. 14, pp. 1286–1289, 2015.

[34] M. Yusop, M. Rahim, M. Ismail, and A. Wahid, "Circular polarization fractal koch microstrip patch antenna using single-fed em coupled ring resonators," in *Proceedings of the 2010 IEEE Asia-Pacific Conference on Applied Electromagnetics (APACE)*, pp. 1–4, IEEE, Port Dickson, Malaysia, November 2010.

[35] V. V. Reddy and N. V. S. N. Sarma, "Compact circularly polarized asymmetrical fractal boundary microstrip antenna for wireless applications," *IEEE Antennas and Wireless Propagation Letters*, vol. 13, pp. 118–121, 2014.

[36] W.-L. Liang, Y.-C. Jiao, L. Zhang, and T. Ni, "Wideband single-feed circularly polarized antenna," *Progress In Electromagnetics Research Letters*, vol. 54, pp. 93–99, 2015.

[37] M. L. Sabran, S. K. A. Rahim, P. J. Soh, C. Y. Leow, and G. Vandenbosch, "A simple electromagnetically fed circularly-polarized circular microstrip antenna," *Applied Computational Electromagnetics Society Journal*, vol. 30, no. 11, pp. 1180–1187, 2015.

[38] T. Jono and K. Jono, "Wideband rectangular printed monopole antenna for circular polarisation," *IET Microwaves, Antennas & Propagation*, vol. 8, no. 9, pp. 649–656, 2014.

[39] A. Panahi, X. L. Bao, G. Ruvio, and M. J. Ammann, "A printed triangular monopole with wideband circular polarization," *IEEE Transactions on Antennas and Propagation*, vol. 63, no. 1, pp. 415–418, 2015.

[40] K. W. Lui, O. H. Murphy, and C. Toumazou, "A wearable wideband circularly polarized textile antenna for effective power transmission on a wirelessly-powered sensor platform," *IEEE Transactions on Antennas and Propagation*, vol. 61, no. 7, pp. 3873–3876, 2013.

[41] T.-C. Yo, C.-M. Lee, C.-M. Hsu, and C.-H. Luo, "Compact circularly polarized rectenna with unbalanced circular slots," *IEEE Transactions on Antennas and Propagation*, vol. 56, no. 3, pp. 882–886, 2008.

[42] K. P. Ray, "Design aspects of printed monopole antennas for ultra-wide band applications," *International Journal of Antennas and Propagation*, vol. 2008, pp. 1–8, Article ID 713858, 2008.

[43] M. S. Ellis, Z. Zhao, J. Wu, X. Ding, Z. Nie, and Q.-H. Liu, "A novel simple and compact microstrip-fed circularly polarized wide slot antenna with wide axial ratio bandwidth for c-band applications," *IEEE Transactions on Antennas and Propagation*, vol. 64, no. 4, pp. 1552–1555, 2016.

[44] M. Midya, S. Bhattacharjee, and M. Mitra, "Triple-band dual-sense circularly polarised planar monopole antenna," *IET Microwaves, Antennas & Propagation*, vol. 13, no. 12, pp. 2020–2025, 2019.

[45] K. Ding, C. Gao, T. Yu, and D. Qu, "Broadband c-shaped circularly polarized monopole antenna," *IEEE Transactions on Antennas and Propagation*, vol. 63, no. 2, pp. 785–790, 2015.

[46] B. Xu, Y. Zhao, L. Gu, C. Huang, and Z. Nie, "Broadband circularly polarized printed falcate-shaped monopole antenna," *International Journal of RF and Microwave Computer-Aided Engineering*, vol. 30, no. 11, Article ID e22395, 2020.

[47] A. A. Althuwayb, M. J. Al-Hasan, A. Kumar, and D. Chaturvedi, "Design of half-mode substrate integrated cavity inspired dual-band antenna," *International Journal of RF and Microwave Computer-Aided Engineering*, vol. 31, no. 2, Article ID e22520, 2021.